Acheron Fossae, Mars: tectonic rifting, volcanism and implications for lithospheric thickness

P. Kronberg, E. Hauber, M. Grott, S.-C. Werner, T. Schafer, K. Gwinner, B. Giese, Ph. Masson, G. Neukum

Acheron Fossae, Mars: Tectonic rifting, volcanism, and implications for lithospheric thickness

P. Kronberg,[1] E. Hauber,[2] M. Grott,[2] S. C. Werner,[3] T. Schäfer,[1] K. Gwinner,[2] B. Giese,[2] P. Masson,[4] and G. Neukum[3]

Received 23 June 2006; revised 16 August 2006; accepted 7 December 2006; published 25 April 2007.

[1] The Acheron Fossae region is an ancient crustal block exposed in the northwestern Tharsis province on Mars. It is named after the Acheron Fossae, a particularly well-developed system of extensional tectonic grabens. This study is the first to describe the tectonic inventory in detail, using topographic and image data from the Global Surveyor and Mars Express missions. We see the extensional tectonics along the east–west trending topographic high of Acheron Fossae as a surface expression of upwelling asthenospheric material that initiated regional uplift, crustal extension and breakup, and associated volcanic activity in Noachian time. The tectonic architecture and the dimensions of the extensional structures are comparable to those of terrestrial continental rifts. An area of elevated topography and strong erosion, which constitutes a regional landmark in the eastern Acheron Fossae region, is interpreted as a rift-related center of volcanism, caused by local magmatic uprise and involvement of the lithosphere. The extension across the Acheron Fossae reaches values between 1.2 km and 8.7 km, comparable to young continental rifts on Earth. Crater statistics indicate an absolute cratering model age between ~3.9 Ga and 3.7 Ga for the rifting. The uplift observed on the flanks of the Acheron Fossae indicates a fairly thin and thus hot lithosphere. Using flexural analysis, we have constrained the elastic lithosphere thickness at the time of rifting to 8.9–11.3 km, corresponding to thermal gradients between 28 and 41 K km^{-1}. These heat flows are substantially larger than Noachian heat flow values previously reported, but are consistent with the presence of rift-related volcanism and a magmatically very active environment.

Citation: Kronberg, P., E. Hauber, M. Grott, S. C. Werner, T. Schäfer, K. Gwinner, B. Giese, P. Masson, and G. Neukum (2007), Acheron Fossae, Mars: Tectonic rifting, volcanism, and implications for lithospheric thickness, *J. Geophys. Res.*, *112*, E04005, doi:10.1029/2006JE002780.

1. Introduction

[2] Rifting on Mars has been the subject of numerous previous publications. Various large graben systems in the Claritas region, in Tempe Terra, and in the Thaumasia province have been discussed as possible rift structures and compared to terrestrial continental rifts [e.g., *Tanaka et al.*, 1991; *Banerdt et al.*, 1992; *Anderson et al.*, 2001; *Hauber and Kronberg*, 2001, 2005]. All these complex extensional features are tens to hundreds of kilometers wide and sometimes more than a thousand kilometers long. They are characterized by several border faults and deep and fractured graben floors, and some of them are associated with volcanic centers. Even the larger Valles Marineris have been ascribed to rift formation radial to Tharsis [e.g., *Frey*, 1979; *Schoenfeld*, 1979; *Masson*, 1977, 1980, 1985; *Wood and Head*, 1978; *Schultz*, 1991; *Anderson and Grimm*, 1998, 1999; *Anderson et al.*, 1999; *Barnett and Nimmo*, 2002; *Komatsu*, 2003]. Rifts are of great interest to studies of the evolution of the Martian crust and lithosphere as well as to models of the thermal evolution, since they are assumed to affect the entire thickness of the lithosphere. The analysis of their morphology and topography can reveal important properties of the lithosphere.

[3] The Tempe Fossae seem to be a viable analogon to a terrestrial continental rift from a geomorphological and structural point of view [*Hauber and Kronberg*, 2001]. The Thaumasia Graben, situated at the western border of the Thaumasia plateau, displays some characteristics that are common to terrestrial continental rifts, whereas other properties are distinctively not rift-like [*Hauber and Kronberg*, 2005]. Results from photogeological mapping of the Coracis Fossae in the Thaumasia region indicate possible rift structures [*Kronberg et al.*, 2006].

[4] In this study, we continue our previous analyses of possible Martian rifts [*Hauber and Kronberg*, 2001, 2005;

[1]Institute of Geology, Clausthal, Germany.
[2]Institute of Planetary Research, German Aerospace Center (DLR), Berlin, Germany.
[3]Institute of Geosciences, Berlin, Germany.
[4]Laboratoire Orsayterre (CNRS FRE 2566), Université Paris-Sud, Orsay, France.

0148-0227/07/2006JE002780

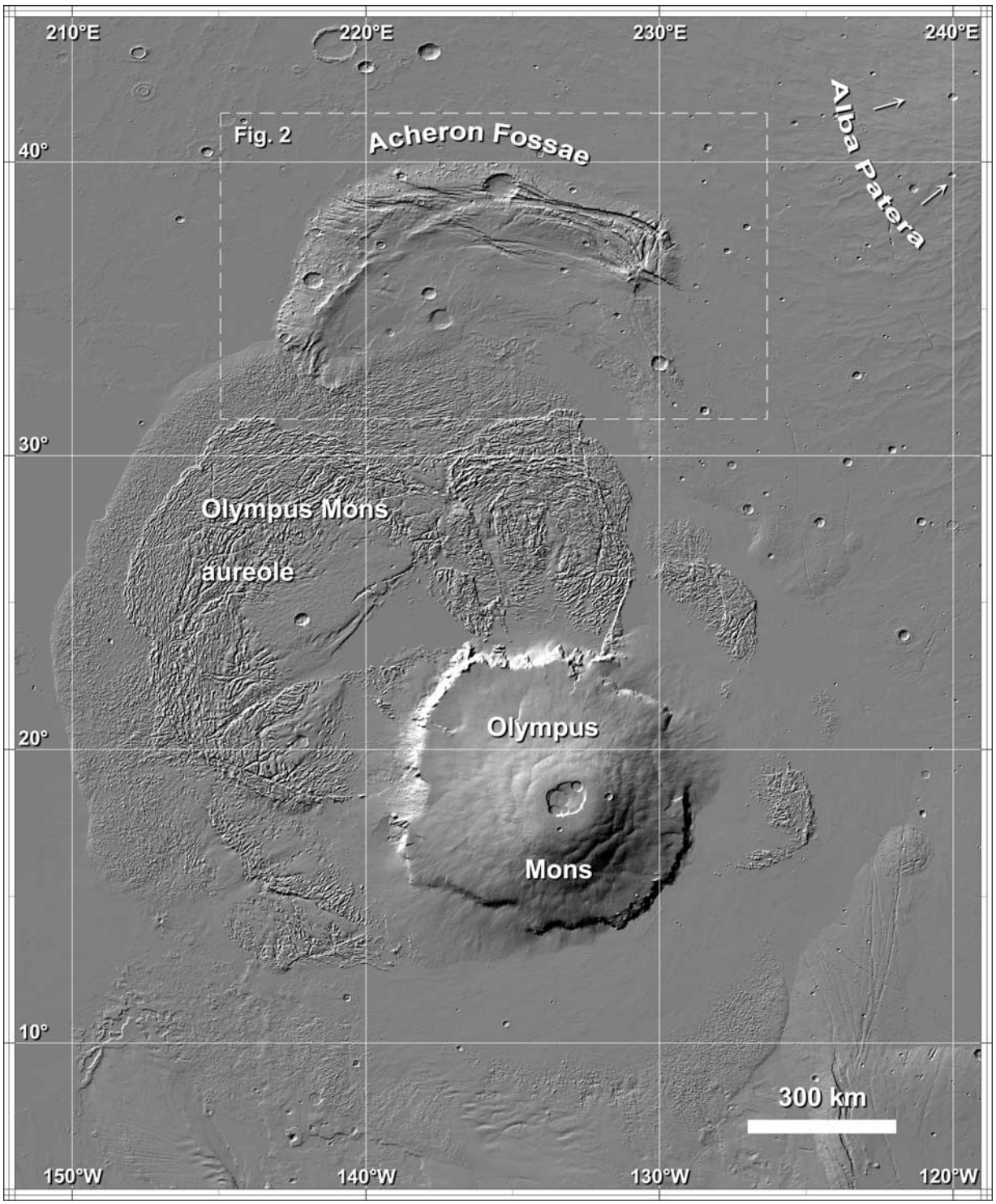

Figure 1. Regional context of the Acheron Fossae region (shaded relief representation based on MOLA data).

Grott et al., 2005; *Grott*, 2005] and focus on the graben system of the Acheron Fossae in northwestern Tharsis (Figure 1). The Acheron Fossae were early recognized as a heavily fractured region [*Scott and Carr*, 1978; *Scott et al.*, 1981; *Tanaka*, 1983], and Viking-based geologic mapping summarized the major geologic surface units of the region [*Morris and Tanaka*, 1994], but no detailed tectonic investigation has been performed yet. We describe their spatial arrangement, their morphology and architecture as well as their style and the degree of extensional deformation, and probably involved magmatectonic processes. Crater counts performed on key areas provide an absolute model age for rift formation. On the basis of rift flank uplift associated with Acheron Fossae, possible values of the

lithospheric thickness at the time of their formation are modeled. We use image data obtained through the High Resolution Stereo Camera (HRSC) [*Neukum et al.*, 2004b] and the Mars Orbiter Camera (MOC) [*Malin et al.*, 1992; *Malin and Edgett*, 2001] for detailed structural mapping. Our topographic measurements were performed on the basis of HRSC stereo images and derived Digital Elevation Models (DEM) [*Scholten et al.*, 2005; *Gwinner et al.*, 2005], as well as on DEM derived from spot elevation measurements by the Mars Orbiter Laser Altimeter [*Zuber et al.*, 1992; *Smith et al.*, 2001].

2. Geography

[5] The Acheron Fossae region consists of an isolated block of ancient terrain situated at the northwestern margin of the Tharsis province. In plan view, it forms an arcuate, north-facing topographic rise, which is about 800 km long and up to 280 km wide. It stands up to 2000 m above its surroundings (Figure 2a). The entire area is a rather isolated geomorphological feature. On a global scale, the most prominent landmarks nearby are Olympus Mons and its aureole to the south, and Alba Patera to the east. For convenient reading, we informally introduce some physiographic names (Figure 2b). The more prominent and older of two rift-like graben systems is called Acheron Fossae 1, the less developed and younger system is called Acheron Fossae 2. An elongated and relatively narrow ''banana''-shaped topographic arch, which extends across the entire block of ancient terrain, is hereinafter referred to as Acheron Dorsum. In its easternmost parts, it widens to a broad dome-like topographic structure, which we name Acheron Montes.

3. Geology

[6] The Acheron Fossae region has been mapped by *Scott and Tanaka* [1986] on a global scale and later by *Morris and Tanaka* [1994] on a regional scale as part of their mapping of the broader Olympus Mons region. Although we expect that the many new data sets that have been acquired since the making of these maps (e.g., MOC and HRSC images) would allow for a more detailed photogeological mapping of the Acheron Fossae, this is beyond the scope of this paper. Therefore we give here an overview of the regional geology based on these previous mapping efforts. In two separate sections on volcanic and glacial or periglacial landforms, we present some of our own geologic observations, which are of importance for the understanding of the geological history of the Acheron Fossae.

3.1. Previous Mapping

[7] The Acheron region has been mapped on the basis of Viking Orbiter images by *Scott et al.* [1981], *Tanaka* [1983], and *Morris and Tanaka* [1994], and more recently with additional MOC, MOLA, and THEMIS data, but on a smaller scale, by *Tanaka et al.* [2005]. It is characterized by a rugged and heavily cratered surface, which was interpreted as ancient volcanic rocks (''fractured unit'' or Naf of the highland materials [*Morris and Tanaka*, 1994]) and a mixture of volcanic and sedimentary material (''Noachis Terra unit'' or Nn [*Tanaka et al.*, 2005]). It was suggested to be of Noachian age [*Scott and Tanaka*, 1986; *Morris and Tanaka*, 1994]. This unit is cut by E–W to ESE–WNW-trending grabens, resulting in a typical horst-and-graben morphology. The bedrock of the units Naf [*Morris and Tanaka*, 1994] or Nn [*Tanaka et al.*, 2005] is incised by many fluvial channels and gullies, which do not extend into the surrounding plains. The grabens and other depressions like craters are filled to varying degrees by material that shows signs of viscous flow and was thought to be of periglacial origin (''smooth materials'', unit Aas of *Morris and Tanaka* [1994]). In the western part of this unit, several rounded hills are located on the outer, NW-facing slopes of the topographic high. They were interpreted as syntectonically active volcanoes, or, alternatively, as remnants of a thick mantle (''mountain unit'' or Nam of the highland materials [*Morris and Tanaka*, 1994]).

[8] The ancient, elevated region is bordered on all sides by younger plains. Toward the south, the plains seem to be mantled by an eolian or pyroclastic deposit (''Plains unit'' or Nap of the highland materials [*Morris and Tanaka*, 1994]). These plains are themselves embayed in the south by the Olympus Mons aureole deposits. In the immediate east, smooth material with lobate scarps and tongue-like flow features were interpreted to be young lava flows of Olympus Mons [*Morris and Tanaka*, 1994]. In the east and northeast, the Acheron Fossae region is embayed by lava flows from Alba Patera, one of the large Martian shield volcanoes. These flows were mapped as lower member of the Alba Patera Formation (Hal [*Morris and Tanaka*, 1994]), In the older map of *Morris and Tanaka* [1994], the plains to the north and west were uniformly mapped as lava flows with an eolian component (''Member 3'' or Aa3 of the Arcadia Formation [*Morris and Tanaka*, 1994]). Later, *Tanaka et al.* [2005] subdivided the plains in four separate units (counterclockwise from northeast to southwest): lava flows of the ''Alba Patera Unit'' (HTa), highly degraded deposits of the geologically complex ''Scandia region unit'' (ABS), sediments of the ''Vastitas Borealis marginal unit''(ABVm), and finally lava and volcaniclastic flows of the ''Amazonis Planitia 1 north unit'' (AAa1n). The main difference between both maps related to these plains is that some of the material bordering the Acheron Fossae on their northern margin is now thought to be of sedimentary, not volcanic, origin, with a significant role of volatiles in their degradation history.

3.2. Volcanism in the Northern Lowlands

[9] The plains to the east, north, and west of Acheron Fossae have been interpreted as mostly lava flows (see previous section), and our observations confirm these notions. HRSC images show clear signs of lava ridges and tube-fed flows as well as flow margins (Figure 3). In several places, low shields with a central summit crater could be observed. Similar shields occur in a variety of locations on Tharsis, for example, in the Syria Planum province and in the southwestern part of Tempe Terra. The margins of the lava plains show an onlap geometry with respect to the topographic high of the Acheron Fossae region. The margin itself is expressed as an upward facing scarp (Figure 4), in agreement with lava flows coming to a halt when they meet the gently rising slope of the rift flank uplift (see section 5). This morphologic expression is not in

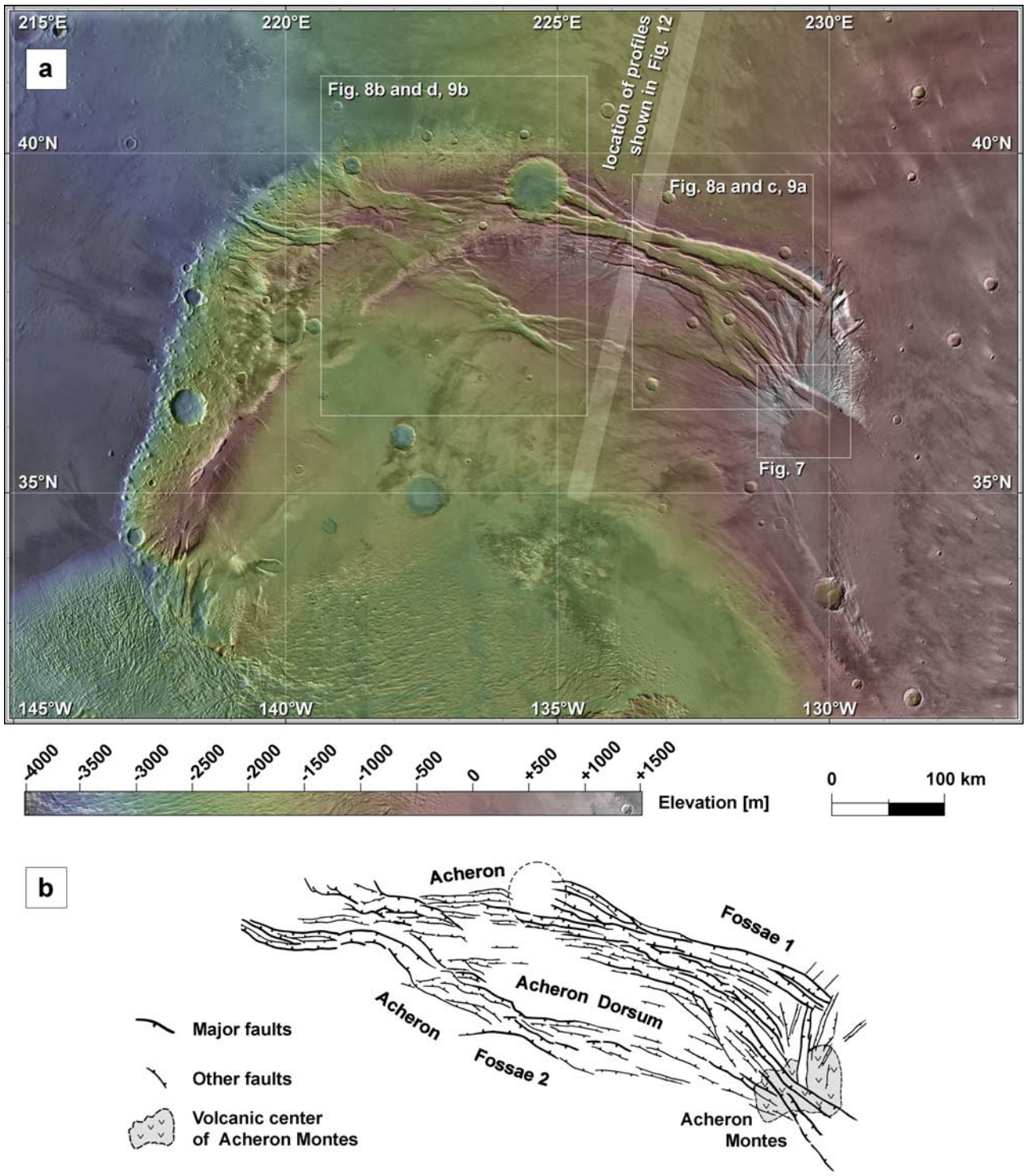

Figure 2. (a) Topographic map of the Acheron Fossae region derived from HRSC-imagery and MOLA topographic data. Location of topographic profiles used for lithospheric thickness modeling indicated by shaded white area. (b) Structural map of the Acheron Fossae graben system and informally introduced physiographic names as used in the text.

agreement with an erosional or constructional shoreline, which has been suggested on the basis of lower resolution Viking Orbiter images at the northern and western border of the Acheron Fossae highland by *Parker et al.* [1989] and *Clifford and Parker* [2001]. While this observation does not exclude an ocean in the northern lowlands, it adds additional weight to the doubts about shorelines raised elsewhere [e.g., *Malin and Edgett*, 1999].

[10] In order to constrain the time of formation of the Acheron Fossae, we determined the absolute model ages of

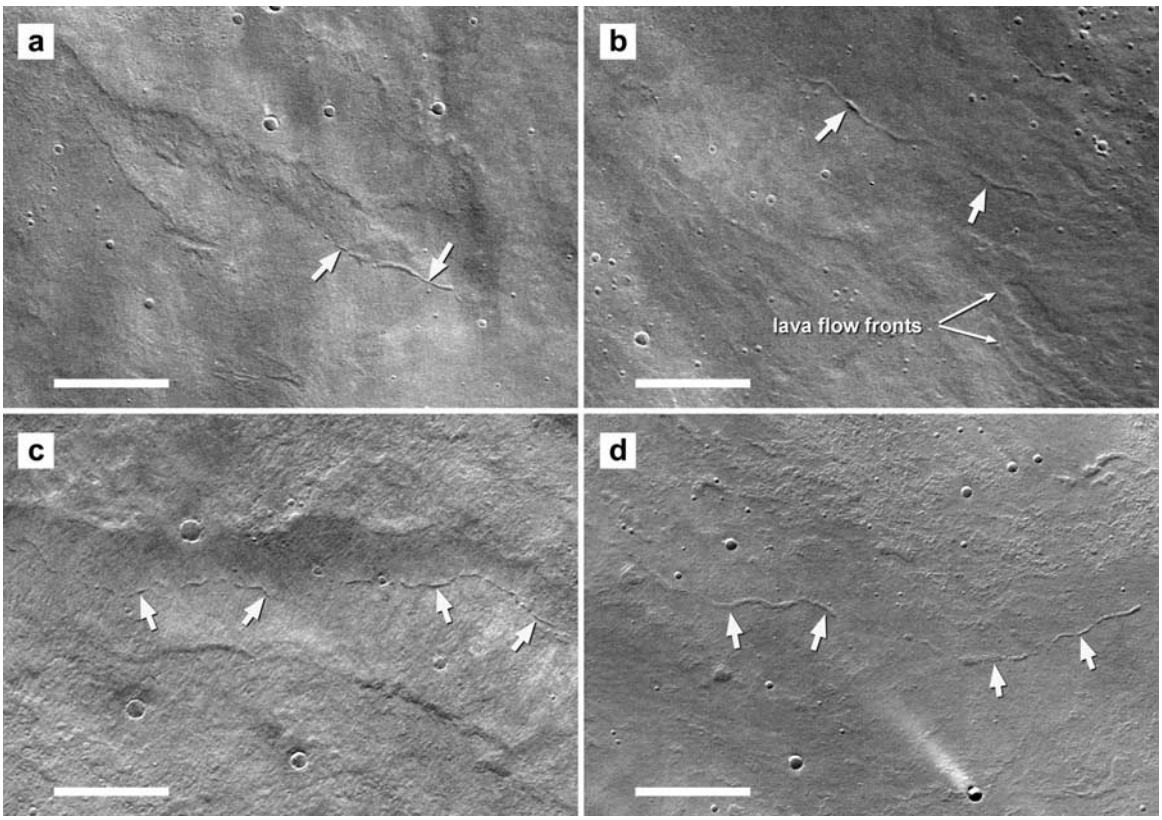

Figure 3. Lava ridges with crestal channels, which are interpreted to be collapsed parts of lava tubes. Lava flow fronts are visible in the lower right part of Figure 3b. Image centers at (a) 42.71°N/229.7°E, (b) 41.07°N/230.06°E, (c) 44.4°N/288.8°E, and (d) 39.39°N/229.97°E. North is up in Figures 3a, 3b, and 3d, north is to the upper left in Figure 3d. The scale bars represent 5 km in all images (Figures 3a, 3b,and 3c: HRSC image 37, Figure 3d: HRSC image 1404).

the volcanic plains surrounding the topographic block of ancient terrain containing the tectonic grabens. The grabens are clearly covered by the plains material, where they run toward the lowlands east and west of the highland block. Therefore they must have been formed before the volcanic plains. We performed crater counts and applied well-established techniques of crater size frequency distribution analysis [*Neukum and Hiller*, 1981; *Hartmann and Neukum*, 2001] to derive absolute model ages. We find that the volcanic plains were formed before 3.75 Ga ($N_{cum}(\geq 1\ \text{km}) = 7.63 \times 10^{-3}$),

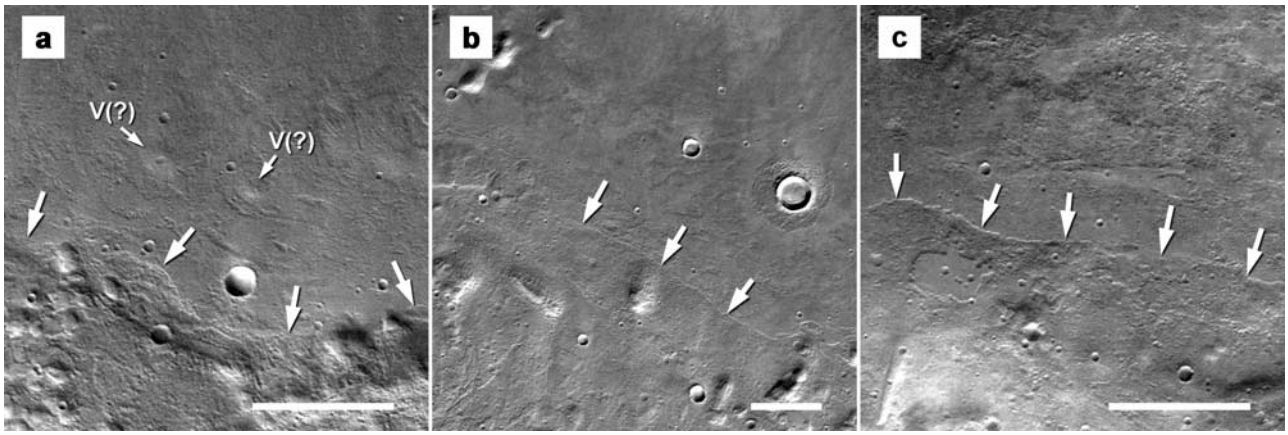

Figure 4. Margins of lava flows embaying the northern flank of the Acheron Fossae region. White arrows mark the upward facing topographic scarp created by the flow fronts of a material with a yield strength (i.e., lava). Letters "V" in Figure 4a mark the positions of possible vent structures. Image centers at (a) 39.72°N/226.82°E (HRSC image 37), (b) 39.84°N/226.24°E (HRSC image 1437), and (c) 39.02°N/228.75°E (HRSC image 1404). In all images, North is up and the scale bars represent 5 km.

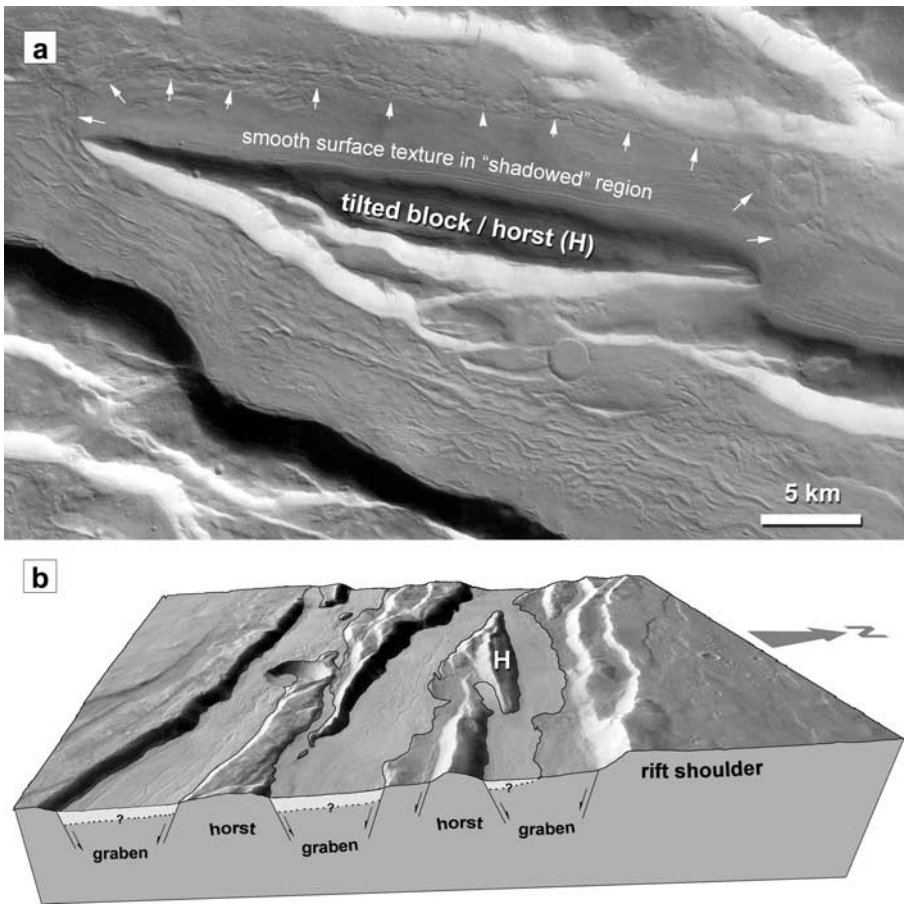

Figure 5. (a) Grabens filled with smooth, young material showing signs of viscous flow. (b) Perspective three-dimensional view of the same area (letter "H" denotes horst in the center of Figure 5a). The distribution of the young mantling material is outlined by solid black lines and bright shading. The depth of the material is unknown, as indicated by dashed lines and question marks (image data and topography from HRSC orbit 37).

and experienced subsequent resurfacing between 3.5 Ga ($N_{cum}(\geq 1\text{ km}) = 3.09 \times 10^{-3}$) to 3.4 Ga ($N_{cum}(\geq 1\text{ km}) = 2.30 \times 10^{-3}$) and locally more recent. These ages are in agreement with the volcanic activity periods of Alba Patera [*Werner*, 2005], and is supported by the geological scenarios as suggested earlier [*Anderson et al.*, 2004; *Cailleau et al.*, 2005]. This coincidence is not surprising, since at least the volcanic plains to the east and northeast of Acheron Fossae had been interpreted to be emplaced by lava flows related to Alba Patera [*Morris and Tanaka*, 1994].

3.3. Glaciers or Rock Glaciers

[11] The Acheron Fossae region is an area of high topographic relief. Like other high-relief regions in the latitude belts of about 30° to 70° north and south [*Mustard et al.*, 2001; *Milliken et al.*, 2003], they display a number of surface features that are indicative of the deposition and degradation of a volatile-rich material in the geologically recent past. Grabens and other topographic depressions like impact craters are filled by a material, which is largely devoid of impact craters and, therefore, seems to be young (Figure 5). At the eastern margin of the Acheron region, it partly fills a large embayment immediately east of the Acheron Montes (Figure 6). It is sometimes very smooth, sometimes rough and degraded, and shows in places signs of viscous flow (Figures 5 and 6). Its distribution seems to be controlled by sun exposure. The southern parts of the W–E-trending grabens, which are more protected from insulation by the steep graben walls, are often covered by this material, while the northern parts do not show this cover (Figure 5). Where the material covers the entire floors of local topographic lows, it seems to be smoother and less degraded in the shadowed southern portions of graben and crater floors (Figure 5). Such a pattern of inhomogeneous distribution is typical for climatically controlled surface deposits. Where it shows a smooth surface texture; that is, where it is not or only weakly degraded, the scarcity of impact craters indicates that it is very young. Since the graben formation took place in the ancient history of Mars (see section 4) and did not extend to the Upper Hesperian or Lower Amazonian (the plains material emplaced in these epochs are not disturbed by faults), it seems that the deposits are not related to the volcano-tectonic history of the Acheron Fossae region. Instead, it shows many, if not all, of the morphological characteristics of material which has been interpreted as rock glaciers [*Squyres*, 1978, 1979; *Lucchitta*, 1984; *Chuang and Crown*, 2005; *Li et al.*, 2005]

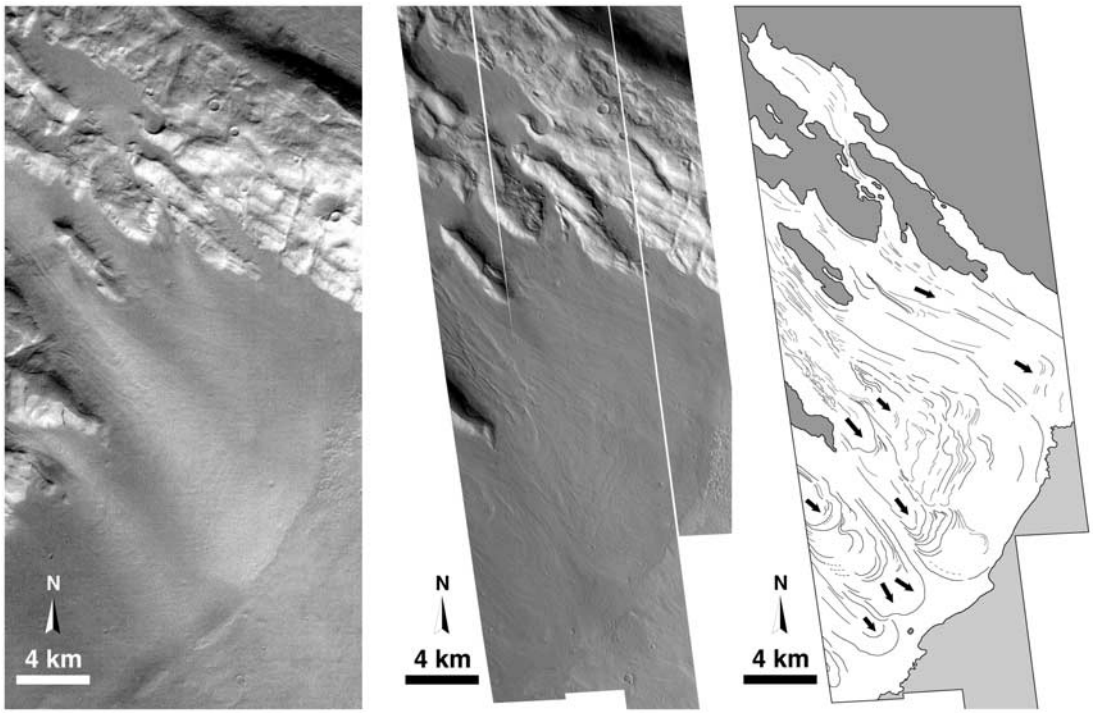

Figure 6. (left) Lobate debris apron at the eastern margin of Acheron Fossae region (HRSC image 1404). (middle) MOC image mosaic of same area, showing the surface texture of the deposit, which might be a rock glacier or a debris-covered glacier (MOC image numbers R03-00521, R03-00873, R03-01181, R03-01562). (right) Geomorphological sketch map, showing evidence for viscous flow.

or debris-covered glaciers [*Hauber et al.*, 2005; *Head et al.*, 2006] in the same latitude belt of the northern hemisphere, where it is mainly found in the fretted terrain at the dichotomy boundary. Indeed, it had been mapped as product of periglacial mass wasting already in the Viking Orbiter-based map of *Morris and Tanaka* [1994]. We agree with these interpretations that this deposit is an originally volatile-rich material probably composed of ice and dust and/or rocks, which was deposited late in Martian history and has since been degraded to varying degrees, depending on its exposition to insulation. While the analysis of this material is not the main focus of this paper, it cannot be neglected either. Since it covers almost all graben floors partly or completely, its thickness masks the true depths of the grabens and, therefore, decreases the measurements of the vertical tectonic displacements. Hence we can not measure the structural throw, but only the observable throw.

[12] At one location at the eastern end of the Acheron Fossae, we made an attempt to estimate the thickness of the viscous material. Here a broad lobe of glacier- or rock glacier–like deposits extends from the Acheron Montes highlands onto the volcanic plains to the east. This pattern is similar to piedmont glaciers at the margin of large ice caps, for example, in Antarctica or in the Canadian Arctic. Topographical profiles derived from HRSC DEM show the shape of the lobate deposit in cross section (Figure 7). Assuming a continuous, flat-lying underground surface, the thickness of the material reaches maximum values of up to 200 m. Since we expect that the underlying surface raises toward the Acheron Montes, this values has to be considered as an absolute maximum, and the real values might be significantly smaller. Since this deposit at the easternmost end of the Acheron Fossae region is one of the largest in the entire region, we do not expect that the thicknesses exceed a few tens of meters elsewhere in Acheron Fossae, and therefore do not significantly affect the extension measurements (see section 4.3).

[13] There is another interesting aspect of the presence of the viscous material in Acheron Fossae. It seems that this material is not restricted to only a few locations on Mars, but seems to be ubiquitous at all longitudes in the two latitudinal belts between $\sim$30° and $\sim$65° north and south. Any predictions of glacier or rock glacier formation by modeling the Martian climate at other obliquities (i.e., other inclinations of the planet's rotational axis with respect to its orbital plane) [e.g., *Forget et al.*, 2006] will have to take this widespread occurrence of these deposits into account.

4. Fault Geometry and Rift Structure

[14] The Acheron Fossae region is situated in the northwestern part of the Tharsis province, about 1200 km north of the large shield volcano Olympus Mons (Figure 1). It is characterized by an arcuate topographic high, which is cut by several complex, $\sim$WNW–ESE-trending tectonic grabens. The dominant morphotectonic feature is a well-exposed rift-like system of horsts and grabens, here named Acheron Fossae 1, that can be traced all over the mountain range (Figures 2a and 2b). Along and across strike, the Acheron Fossae 1 display major changes in their width and structural setting. The width of the rift narrows down westward. The overall elevation decreases from altitudes

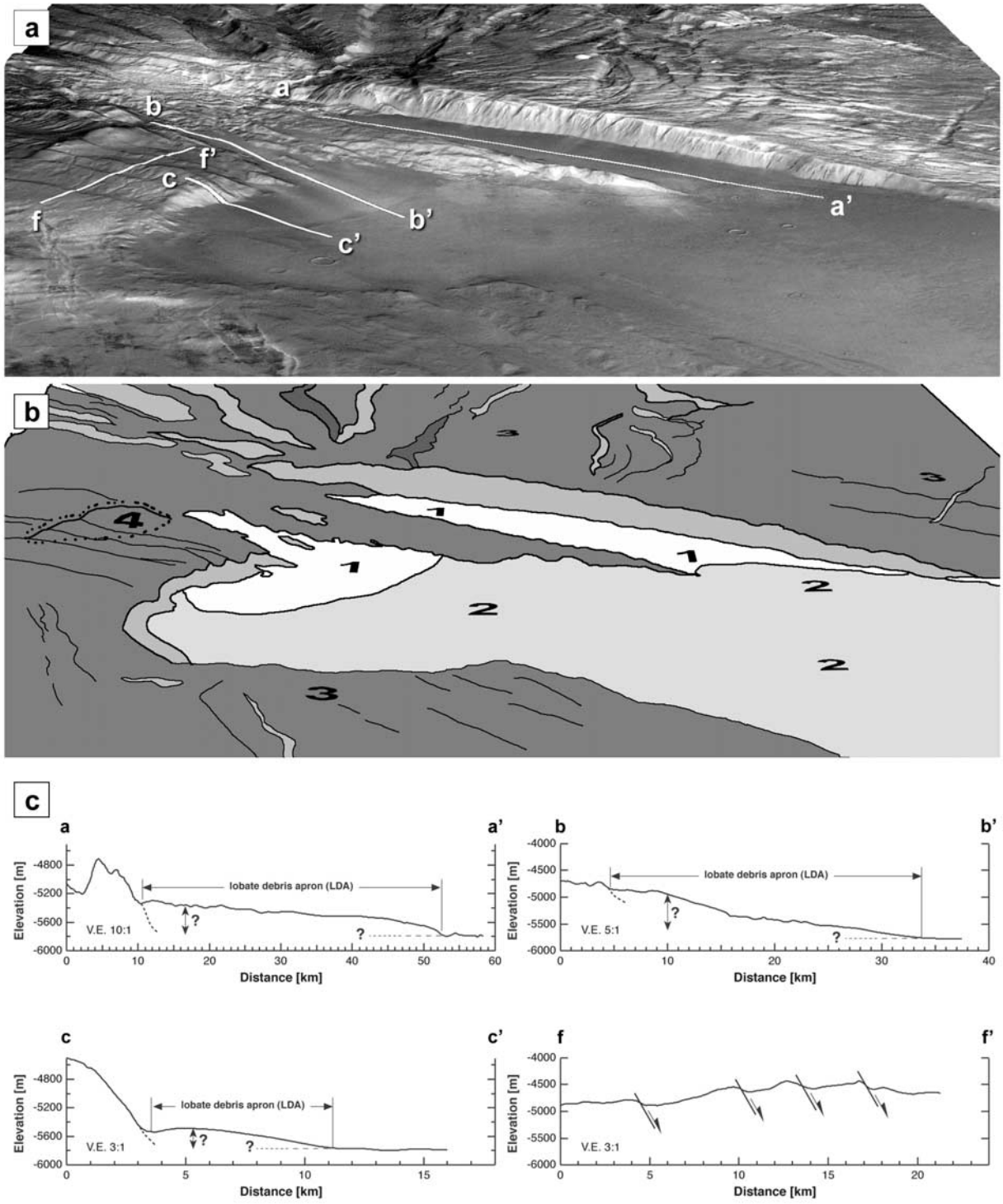

Figure 7. (a) NW-looking, perspective three-dimensional view of eastern margin of the Acheron Fossae region. The location of the profiles a-a′, b-b′, c-c′ and f-f′ in Figure 7c is indicated by solid white lines. (b) Geomorphological sketch map. Unit 1, smooth unit showing viscous flow (compare with Figure 6) and a close similarity to lobate debris aprons thought to be rock glacier-like deposits [e.g., *Squyres*, 1978]; Unit 2, lava flows embaying the high topography of the Acheron Fossae region (e.g., from Alba Patera); Unit 3, ancient crustal material of the Acheron Fossae region; Unit 4, small volcanic edifices associated with the Acheron Montes volcanic rise (see Figure 11). (c) Topographic profiles from high-resolution HRSC Digital Elevation Models. a-a′, b-b′, and c-c′ are profiles crossing the fronts of lobate debris aprons. The thickness is unknown, but assuming a more or less flat preexisting surface it might reach values of >100–200 m. f-f′ is NE-dipping step faults cutting the small volcanoes shown in Figure 11. Images and topography are from HRSC image 1404.

of around 2000 m in the eastern rift segments to values of around −3000 m, where the extensional fault system disappears under the younger lowland cover. A local topographic high with altitudes of around 500 m characterizes the western Acheron Fossae. The general morphology of the Acheron Fossae region indicates crustal upwarping. The slope of the northern flank reaches 3.0°. The southern flank shows values between 1° and 1.5°. The shoulders of the northern graben system are elevated, indicating flank uplift (see section 5.1). A topographic high, here called Acheron Dorsum, about 280 km long, around 100 km wide and up to 1450 m high, forms the southern flank of the proper Acheron Fossae 1 rift system along its central segment. To the south, Acheron Dorsum is bordered by an en echelon system of smaller grabens, which marks the limit of the Acheron Fossae 1 extensional system.

[15] A regional landmark of the eastern Acheron Fossae 1 is a topographic rise, here named Acheron Montes (Figures 2a and 2b). With altitudes up to 3235 m, it is located inmidst the eastern horst and graben series and crossed by graben structures (see Figure 2b). We interpret this topographic rise as a rift-related center of volcanic activity. Toward southeast, the Acheron Fossae mountain range ends with a rather abrupt morphological break.

[16] The morphology of the western mountain range is characterized by a complex system of northwest–southeast trending major grabens, which we informally refer to as Acheron Fossae 2 (see Figures 2a and 2b). Its predominant morphotectonic features are two large sinuous grabens separated by an extensive horst structure and crossing a local topographic high. Toward southeast, the double graben system develops into an single graben that borders the southern flank of Acheron Dorsum and continues southeastward until it disappears under volcanic flows and eolian deposits. Altogether, the northwest–southeast trending Acheron Fossae 2 system can be observed over a length of about 430 km. The width of the double graben in the west varies between 50 and 75 km, and that of the single graben in the east from 10 to 35 km (Figures 2a and 2b). As shown in Figure 2b, E–W-trending horst-and-graben structures of the Acheron Fossae 1 system are crossed obliquely by graben structures of the Acheron Fossae 2. The vertical displacement reaches up to 1100 m of observable throw on the southwest dipping Acheron Fossae 2 border faults.

4.1. Acheron Fossae 1

[17] The HRSC anaglyph image (Figure 8a) provides a synoptical view of the topography and structural setting of the eastern Acheron Fossae 1 as well as insight into the three-dimensional properties of its extensional fault system. A few extensive steep normal faults with large observable throw outline the horst and graben architecture of the arcuate rift segment (Figure 8b). The surface slopes across the faults are moderate and reach maximum values between 30°–40°. This is close to the angle of repose and seems to be an effect of erosion, as indicated by debris at the base of the fault scarp. Therefore we interpret the fault dip to be steeper. Individual curvilinear grabens are 10–20 km wide and can be traced over a length of up to 170 km. The length of segmented border faults varies between 30 km and 80 km. Rift width and rift architecture change along the trend of the rift: A zone of complex extensional structures (lower left) and a width of about 140 km narrows down to an internally faulted rift graben (upper right) of 45 km width.

[18] The change in structural morphology and related rift architecture along the rift trend is illustrated by three topographic profiles derived from HRSC data (Figure 9a). Profile 9C displays crustal upwarping and the architecture of the 45-km-wide rift valley. Its three internal grabens (each about 10 km wide) are separated by intermediate horst structures (6–7 km wide). Step faults modify the extensional faulting, and graben floors are tilted by a few degrees. The observable displacement at the northern border fault system is about 1250 m, as compared to 715 m offset at the southern border fault. The elevation of the southern rift shoulder reaches 1470 m, that of the northern rift shoulder 1170 m. The topography of the rift shoulders indicates flank uplift on both rift flanks. The slope of rift flanks varies between 2° and 2.5°. The depth of graben floors reaches ∼1060 m for the axial graben and ∼600 m for the tilted floor of the southern graben.

[19] HRSC DEM and corresponding orthoimages can be used to render perspective views of selected areas. Figure 10 displays the morphology and structural setting of the above described part of the Acheron Fossae 1 system in a eastward looking perspective view. It also reveals that graben floors can be covered by late deposits of various origin (see section 3.3). With regard to the displacement values along the rift system, one has to keep in mind that rift floors and step fault platforms are often covered. Therefore the displacement values given in this text indicate the minimum displacement of mapped faults though we do not expect the cover to be thick enough to significantly change the values for fault offsets.

[20] The morphotectonic units and the style of extensional deformation across the 140-km-wide southeastern segment of Acheron Fossae 1 are displayed in profile a-a′ in Figure 9a. HRSC data show 2040 m of vertical throw on the northern border fault. Again, the topography of the northern rift shoulder indicates flank uplift. A slope of 3° toward NE has been determined for the northern rift flank. The internal structure of the northern graben is characterized by two 6-km-wide grabens separated by a 7.5-km-wide intermediate horst block with ∼1060 m and 920 m offset on its southern and northern master faults, respectively. A vertical offset of 1580 m is observable on the southern border fault of the northern graben. Toward the south, an outstanding horst structure is about 30 km wide. A vertical offset of 1200 m on its steep southern border fault results in a general step-down in overall elevation of the adjacent series of multiple horsts and grabens. A 10-km-wide graben is located in front of the steep southern border fault system of the eastern rift valley. The latter shows 1440 m of vertical throw. The elevation of the rift shoulders varies between ∼950 m at the southern rift flank and ∼1830 m at its northern counterpart.

[21] The easternmost rift segment is located on a topographic high, which we informally refer to as Acheron Montes (Figure 2b). It reaches an altitude of 3225 m and resembles morphologically similar structures that have been interpreted as ancient Noachian-aged volcanoes in the Tempe and Thaumasia regions [*Scott*, 1982a, 1982b]. Characteristical properties of the volcanic edifices in the Thaumasia region in southeastern Tharsis are outlines that are

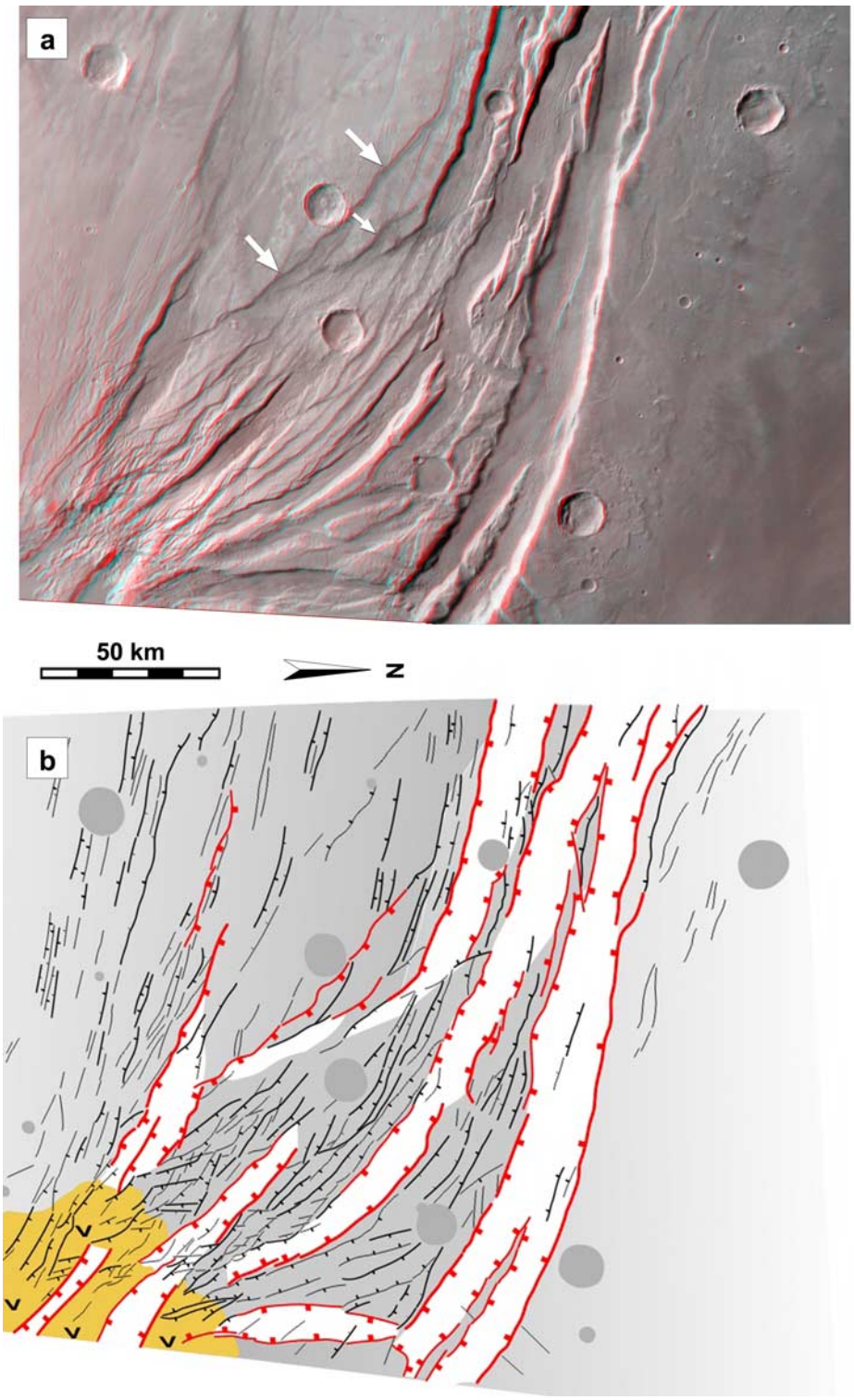

Figure 8. (a) HRSC anaglyph image (orbit 0037) showing topography and crustal extension of the eastern Acheron Fossae 1. Owing to the almost polar orbit of HRSC and the forward and backward looking geometry, North is to the right (use red-blue glasses for three-dimensional viewing, red glass on the left eye). (b) Structural map of the eastern Acheron Fossae 1. Main border fault systems are shown in red, outlining large graben structures. V-shaped symbols and yellowish color show larger parts of Acheron Montes, a rift-related center of volcanic activity. (c) HRSC anaglyph image (orbit 0143) showing topography and crustal extension of the western Acheron Fossae area. Note superposition and vertical displacement of Acheron Fossae 1 structures by Acheron Fossae 2 graben (north is to the right). (d) Structural map of the western Acheron Fossae area. Main border fault systems are shown in red and outline large grabens of the Acheron Fossae 1 and 2 structures.

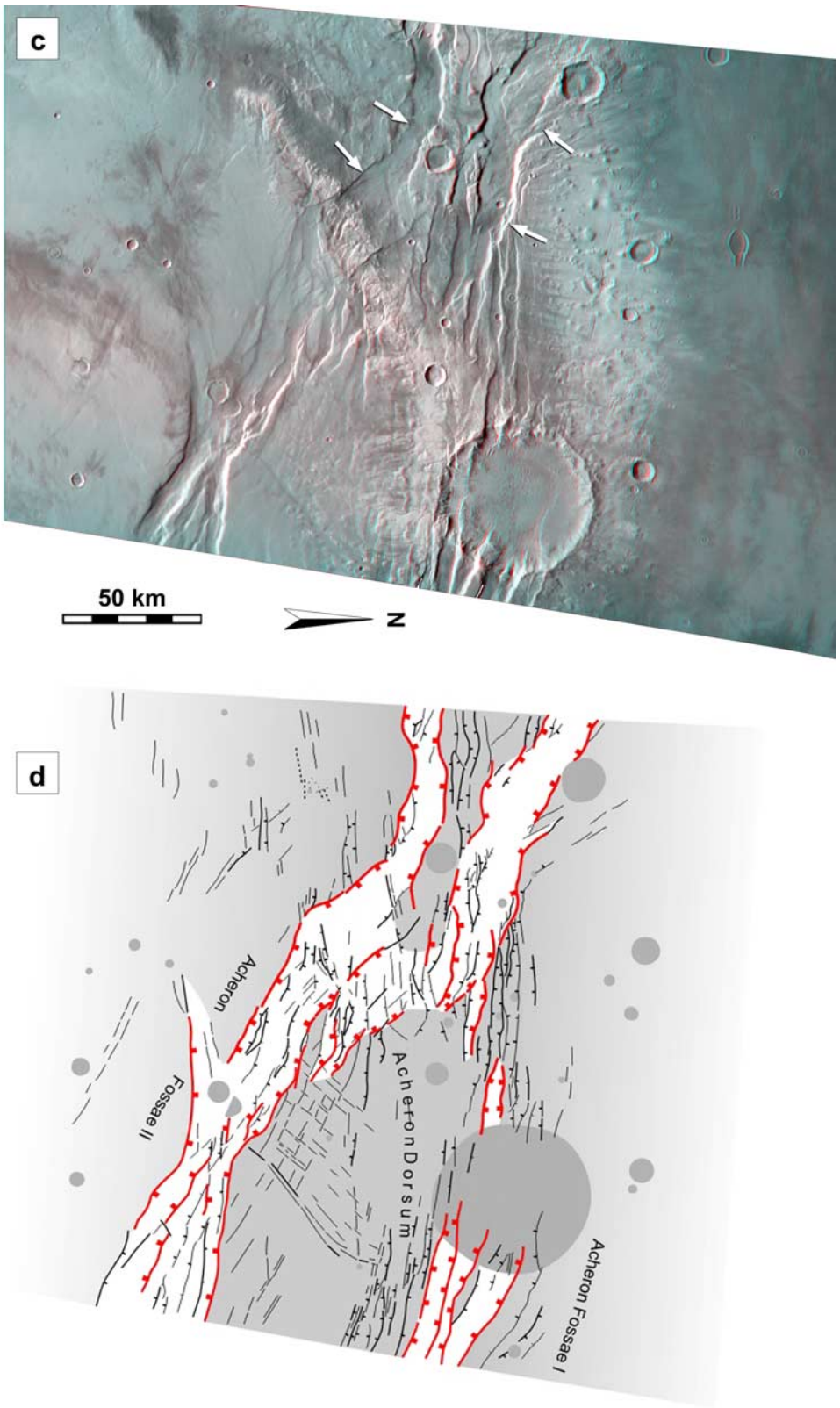

Figure 8. (continued)

circular or elliptic in plan view, and heavily eroded flanks, often dissected by radial patterns of fluvial channels. A typical example is situated at the eastern Coracis Fossae, an old rift in Thaumasia [*Kronberg et al.*, 2006; *Grott et al.*, 2005, Figure 1]. Therefore we believe that the topographic rise of Acheron Montes represents a rift-related center of volcanic activity associated with local magmatic uprise. This is confirmed by HRSC topographical data and the observed tilt of the graben floors of the eastern rift segment. They show an increase in overall elevation of rift structures

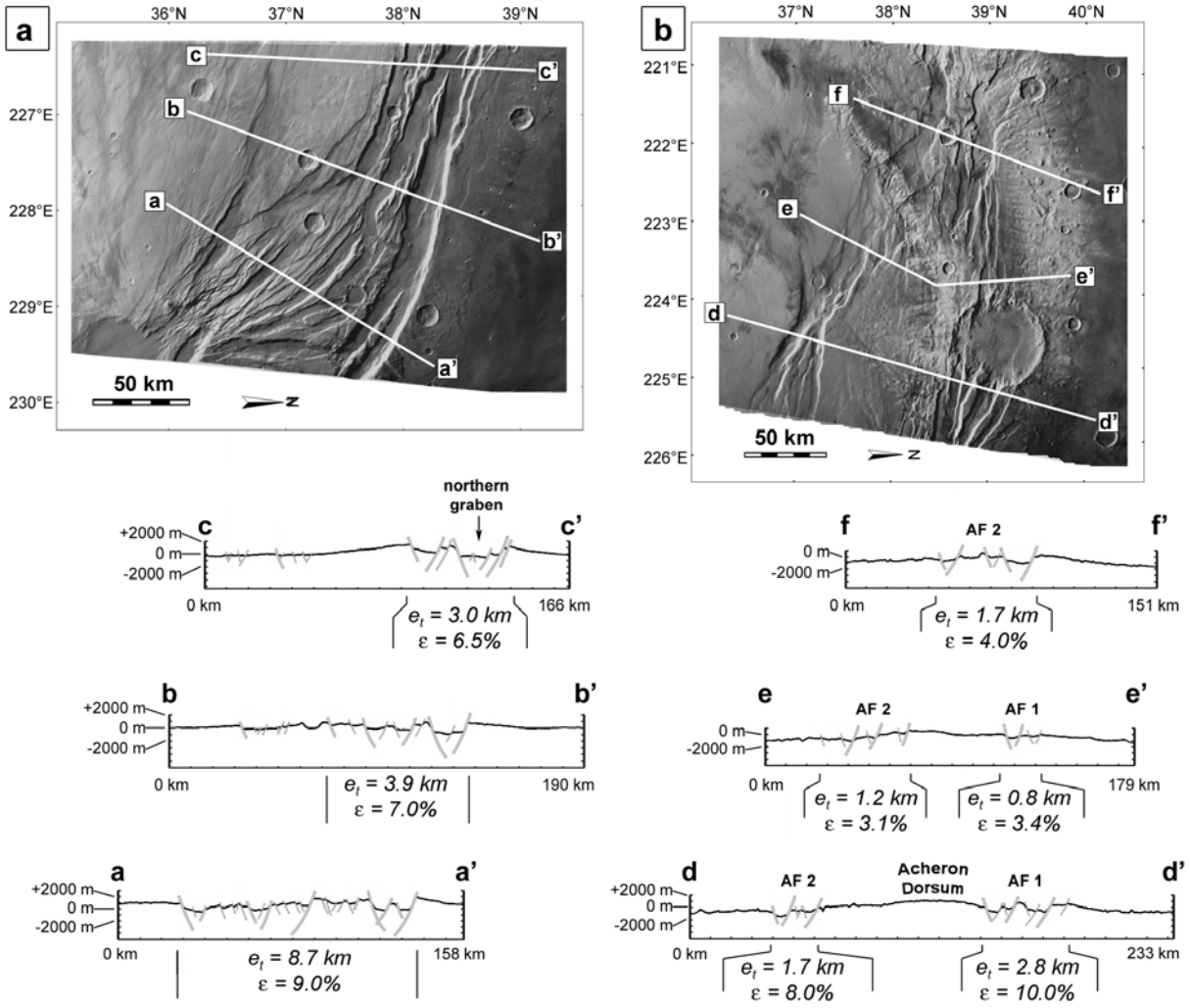

Figure 9. (a) Graben architecture according to representative MOLA profiles and inferred fault systems of the eastern Acheron Fossae 1 (HRSC image 37; note that north is to the right for better comparison to Figure 8). a-a′, b-b′, and c-c′: topographic profiles across the rift system (main faults are shown with thick, solid gray lines). Numbers indicate measured crustal extension (e_t) and corresponding strain (ε). (b) Same for the western Acheron Fossae area (HRSC image 143).

with decreasing distance toward the center of Acheron Montes while the observed northwestward dip of major graben floors steepens from an average of 1.5°–2° to 10.5° near the center of Acheron Montes. The suspected volcanic rise is crossed and faulted by a 35-km-wide southeast-trending graben system, indicating an early to synrift age of volcanic activity.

[22] Near the center of Figures 8a and 8b, a steep normal fault system running oblique to the general rift trend and dipping northeast (upper left) marks the border between the eastern rift segment and Acheron Dorsum. Step faults associated with this ~100-km-long fault system displace the eastern horst and graben series by about 1100 m, creating a topographic low in front of the fault zone (compare Figure 2). The location and development of the oblique fault system and the associated topographic low could be related to magma withdrawal toward the Acheron Montes volcanic rise.

4.2. Acheron Fossae 2

[23] An HRSC anaglyph (Figure 8c) provides a synoptical view of the topography of the western Acheron Fossae mountain range. At the same time it provides three-dimensional information on the spatial occurrence and the fault geometry of the Acheron Fossae 2 graben system, as well as on the crosscutting relationships between the Acheron Fossae 1 and 2 extensional fault systems. As already mentioned, the Acheron Fossae 2 graben are superimposed on the Acheron Fossae 1 rift system. The observable change in the directional trend of individual grabens and their border fault systems as well as oblique internal block-faulting of individual grabens both suggest a reactivation of preexisting Acheron Fossae 1 structures and their influence on the development of the Acheron Fossae 2 grabens (see Figures 8b and 8d).

[24] In its northwestern segment (upper (= western) half of Figures 8c and 8d), the Acheron Fossae 2 system is

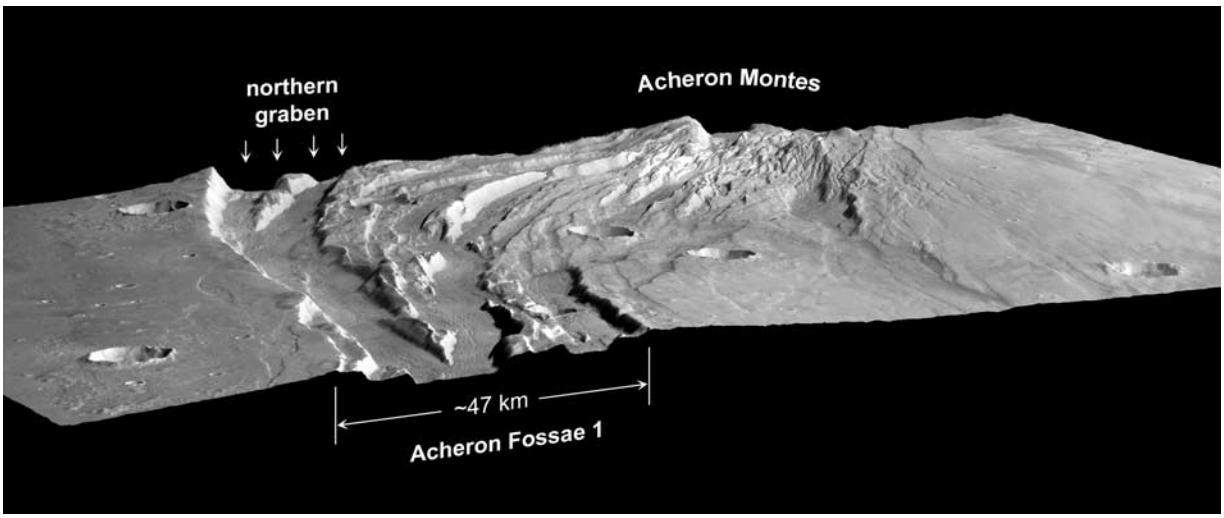

Figure 10. Eastward looking perspective three-dimensional view showing morphology and structural setting of the southeastern parts of the Acheron Fossae 1 and Acheron Montes, a rift related center of volcanic activity (HRSC image 0037).

characterized by two sinuous grabens. Their observable lengths are around 200 km and 230 km, and the widths reach 12 km and 20 km. They are separated by an intermediate 10- to 40-km-wide horst block, and are associated with a topographic and structural high (see Figure 2a). The length of the border faults varies from 15 to 35 km. The largest vertical throw is observed on south-dipping border fault systems (compare the topographical profiles in Figure 9b). Accordingly, southern graben shoulders generally display lower elevation than their northern counterparts.

[25] The south-dipping master fault system of the northern graben, which cuts and displaces Acheron Fossae I structures, shows up to ~1400 m of vertical displacement. Along the southern border fault of the intermediate horst block, the observable throw reaches about 1150 m.

[26] The double graben is situated on a local topographic high about 100 km in diameter. Tilted graben floors as well as the horst surface are dipping away from it (see Figure 9b, profile f-f′). The topography might indicate local crustal upwarping due to small diapiric magmatic uprise.

[27] A morphological step marks the transition from the double graben system into the single graben as shown in Figures 8c and 8d. The step occurs where the extensional system crosses a light-toned lithological series. Here the latter is faulted into two larger crustal blocks, about 28 km and 22 km wide and displaced stepwise northwestward by 310 m and 420 m, respectively.

[28] The double graben system narrows southeastward (toward lower right) and develops into an asymmetric step-faulted graben, 10–20 km wide and with an observable length of 200 km (see Figure 2a). Again, the largest throw does occur on southwest-dipping border faults (see profiles , d-d′ and e-e′ in Figure 9b). More than 1400 m of vertical displacement is observed along the southwest-dipping fault system bordering Acheron Dorsum, and 350–660 m on its northeast-dipping counterpart. Generally, the larger southward slip on southwest-dipping normal faults results in a drop of the overall elevation along the southwestern flank of the Acheron Fossae 2 graben system.

4.3. Rift-Related Surface Ages

[29] In order to better understand the period of rift formation, crater frequencies were measured for key areas in the Acheron Fossae region. On the basis of HRSC imagery, parts of the north-facing rift flank (Acheron Fossae 1) and a few horst segments were selected to determine absolute ages. Naturally, these areas are quite small and allow for very few large remaining craters only. Nevertheless, these measurements resulted in a surface age range of 3.9 ± 0.05 Ga ($N_{cum}(\geq 1$ km) = 2.95×10^{-2} to 1.53×10^{-2}). The embaying volcanic units (see section 3.2) could have formed immediately after the formation of the grabens. Their surface ages imply that they were emplaced no earlier than 3.75 Ga ago, and later further volcanic resurfacing events occurred about 3.5 Ga ago and locally even later. These surface ages are in agreement with earlier results and represent the time frame for the tectonic activity in the Acheron Fossae region.

4.4. Extension

[30] In order to determine the amount of crustal extension and the corresponding strain, we performed topographic measurements along several HRSC topographic profiles across the eastern rift segment (see Figure 9). HRSC data allow precise depth measurements of grabens. The fault dip α of normal faults was assumed to be 60°, indicated by rock mechanics [*Anderson*, 1951] and previously used by other authors measuring extension on Mars [e.g., *Banerdt et al.*, 1992, and references therein; *Schultz*, 1995; *Golombek et al.*, 1996; *Mège and Masson*, 1996; *Harrington et al.*, 1999]. Total or cumulated extension e_t along a profile is given by

$$e_t = D_t / \tan \alpha, \tag{1}$$

where D_t is the cumulated vertical offset at faults identified in high-resolution HRSC images of orbit 037 (30 m/pixel). Strain ε is determined from the length of the profile after

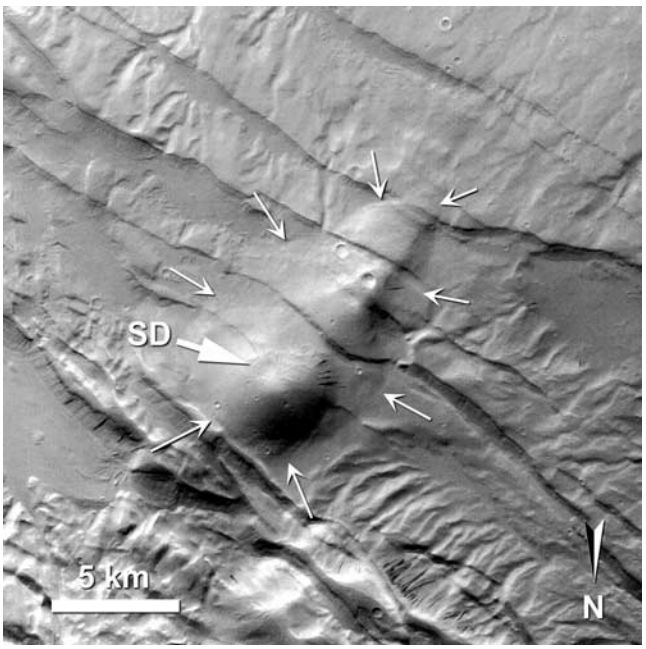

Figure 11. Small volcanic domes in the Acheron Montes volcanic region (HRSC image 1404). The edifices are cut by faults (see profile F-F′ in Figure 7c), indicating that the tectonic activity continued after their formation was largely completed.

extensional deformation (L_{final}) and the length of the profile before extensional deformation ($l_0 = L_{final} - e_t$) by

$$\varepsilon = \left(L_{final} - l_0\right)/l_0. \quad (2)$$

[31] Figure 9a shows the location of profiles and values obtained from HRSC topographic data for the central and eastern Acheron Fossae 1 rift segments. Across the area shown in Figure 9a, the extension values change from 3.0 km to 8.7 km from the 45-km-wide rift valley into the 150-km-wide zone of multiple faulting. At the same time, strain values vary between 6.5% and 9%. Measurements across profile c-c′ and b-b′ in Figure 9 show that crustal extension is accommodated by 52% and 63%, respectively, by a few master faults with large observable throw. Across profile a-a′, large normal faults contribute 44% of crustal extension.

4.5. Rift-Related Volcanism

[32] As shown in Figure 10, the topographic high of the Acheron Montes is a predominant feature of the eastern Acheron Fossae 1 rift system. Situated in the eastern rift segment, it is crossed and faulted by southeast-trending rift structures (see above). Comparative photogeological studies show that the location, morphology, and structural features of the topographic high are comparable to the topographic and structural appearance of two rift-related volcanoes of the Coracis Fossae rift system as mentioned by *Grott et al.* [2005].

[33] Two small volcanic domes are superposed on the larger volcanic massif of the Acheron Montes (Figure 11). Together they form a slightly elongated, NE-trending ridge about 12 km long and 7.5 km wide. The larger of the two edifices reaches a height of about 1000 m above the surrounding terrain. The flank slopes of these constructs have maximum values of more than 25°, but generally they are below 20°. The larger dome shows a summit depression, which might correspond to a volcanic summit crater. We interpret these features to be small shield volcanoes or, alternatively, cinder cones, since the observed steepness of the flanks does not rule out one or the other possibility.

[34] The entire elongated small volcanic rise is cut by NW-trending normal step faults dipping toward NE. This again indicates that the volcanic activity had its major phase before or during the faulting, but that faulting continued after the end of volcanism.

[35] There are other landforms in the Acheron Fossae region that have been interpreted to be volcanic in origin, which are not the focus of our paper, but are shortly discussed here. Diacria Patera is a degraded circular depression with a diameter of about 60 km, which is centered at 34.8°N and 227.3°E. It was described as an ancient shield volcano similar to those in the southern highlands, for example, Hadriaca and Tyrrhena Paterae. HRSC images do not show any evidence for a volcanic origin, and an impact origin seems plausible. The ''banana-shaped'' topographic high displays a large rift-like depression along its crest, which might represent a volcanic fissure [*Morris and Tanaka*, 1994]. It should be noted that numerous small hills on the outer western flank of the Acheron Fossae region have been interpreted as volcanic edifices by *Morris and Tanaka* [1994]. However, HRSC images of these mounds do not show any evidence for a volcanic origin.

5. Elastic Thickness and Heat Flow

[36] To determine the elastic thickness of the lithosphere at the time of rift formation, we have taken 16 topographic profiles in the shaded region indicated in Figure 2. They are given in Figure 12, where subsequent profiles have been offset by 1000 m for better readability and south is on the left. The flank uplift is very pronounced, the rift shoulders

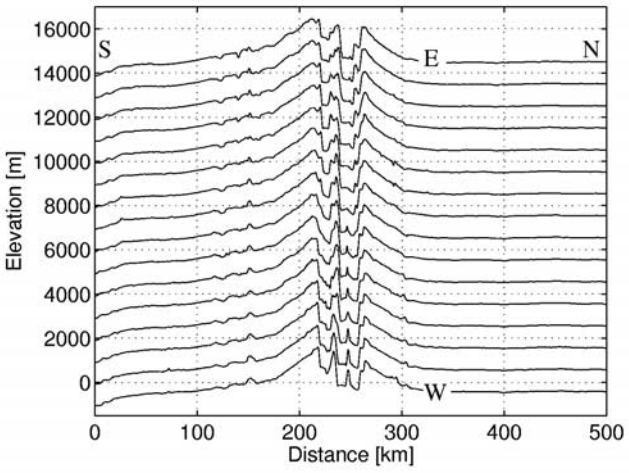

Figure 12. MOLA topographic profiles taken in the shaded region indicated in Figure 2. For better readability, subsequent profiles have been offset by 1000 m. South is on the left and the east-most and west-most profiles have been labeled by 'E' and 'W', respectively.

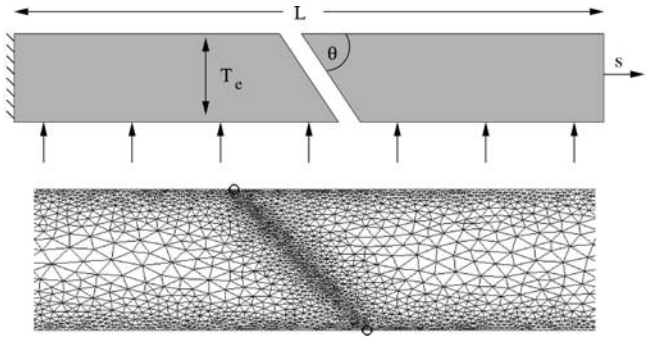

Figure 13. (top) Schematic setup of the finite element model. The plate of length L and thickness T_e is fixated at the left edge while the right edge is extended horizontally by an amount s. The model fault is implemented as a 1-m-wide gap (greatly exaggerated) of large stiffness, cutting the plate at an angle $\Theta = 60°$. Restoring forces are applied at the base of the plate. (bottom) Finite element grid is in the vicinity of the fault; the fault tips are indicated by circles.

standing more than 1000 m above the surrounding planes. On the southern side the rift flank uplift is overprinted by a global topographic decline of $\sim$5 m km^{-1}. This gradient needs to be removed for the geophysical modeling as the part of topography caused by rift flank uplift vanishes for large distances.

[37] The uplift observed on the flanks of the Acheron Fossae rift system may be explained in terms of the isostatic rebound of the lithosphere, a reaction to the unloading associated with extension. The lithospheric flexural strength largely controls amplitude and wavelength of the resulting deformation [*Weissel and Karner*, 1989; *Chéry et al.*, 1992] and estimates of the elastic lithosphere thickness T_e may be obtained by modeling the uplift [*Upcott et al.*, 1996; *Brown and Phillips*, 1999; *Grott et al.*, 2005].

[38] We use the plane strain application mode of the commercial finite element package FEMLAB (http://www.femlab.com) to solve for the displacements resulting from extension and isostatic rebound. They are calculated assuming values for Young's modulus and Poisson ratio of 80 GPa and 0.25, respectively [e.g., *Schultz and Watters*, 2001; *Watters et al.*, 2002]. The Martian surface gravity is 3.72 m s^{-2} and the mantle density is 3500 kg m^{-3} [*Sohl et al.*, 2005]. The model setup is given by an elastic plate of length L and thickness T_e, dissected by a model fault (Figure 13, top). The faulting angle is 60°, corresponding to a frictional parameter of 0.6, a value typical for crustal rocks on Earth. The length of the plate is chosen such that vertical displacements are negligible at the plate boundaries and we adopt L = 1000 km. The left edge is constrained to zero horizontal displacement, while the right edge is extended by an amount s. The restoring force due to buoyancy is applied at the base of the plate, having stiffness $\rho_m g$, where ρ_m is mantle density and g gravitational acceleration. A body load of $\rho_c g$ has been applied, where the plate is in a lithostatic state of stress and the crustal density ρ_c is 2800 kg m^{-3} [*McGovern et al.*, 2004].

[39] The fault is implemented by a 1-m-wide gap with large gap stiffness to prevent the hanging wall and footwall from separating from or passing through each other. As we do not model stick-slip behaviour, friction on the fault is disregarded. The two-dimensional finite element grid is shown in the bottom of Figure 13 and consists of approximately 25,000 elements, which are refined at the boundaries, the maximum element size being 1 km at the upper and lower boundaries and 500 m at the fault surfaces.

[40] To relate the elastic thickness to the mechanical and thermal structure of the lithosphere, we apply the strength envelope formalism of *McNutt* [1984]. Assuming a linear temperature increase with depth, the mechanical thickness of the lithosphere T_m may be calculated. Furthermore, given the curvature K of the flexed lithosphere, the bending moment M_{YSE} is obtained by integration. The elastic thickness T_e corresponding to K and M_{YSE} is then given by

$$T_e = \left(\frac{12(1-\nu^2)M_{YSE}}{KE}\right)^{\frac{1}{3}}. \quad (3)$$

Mueller and Phillips [1995] have shown by numerical experiments that reliable results for the mechanical thickness are obtained if the maximum curvature of the fitted plate is substituted for K. Then a diagram relating T_e, T_m and K may be used to determine T_m and the associated thermal gradient $\frac{dT}{dz}$. We adopt a strain rate of 10^{-16} s^{-1} [*Grott*, 2005] and a surface temperature of 220 K. The brittle portion of the strength envelope is defined using the relations by *Mueller and Phillips* [1995], which are based on Byerlee's law [*Byerlee*, 1978]. Ductile deformation in the crust is governed by a diabase flow law [*Caristan*, 1982].

6. Modeling Results

[41] The calculations have been carried out for elastic thicknesses between 2 and 30 km and extension s between 500 and 4500 m. The best fit was determined by calculating

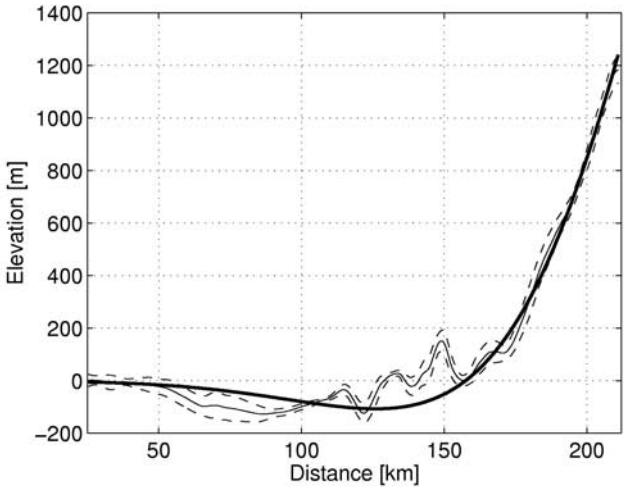

Figure 14. Mean topography as a function of distance along profiles for the southern rift flank, obtained by stacking the profiles shown in Figure 12 (solid line). The spread of 1 standard deviation is indicated by dashed lines and results have been smoothed with a moving average; the smoothing length is 5 km. The best fit FEM profile is given by the bold line.

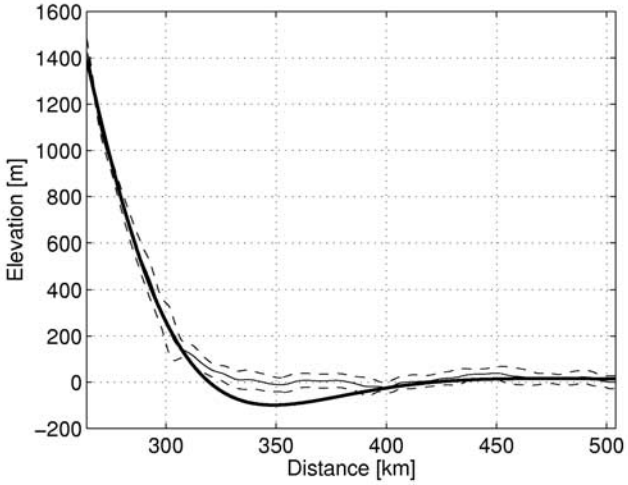

Figure 15. Same as Figure 14, but for the northern rift flank.

the l^2-norm of the difference between the flexure profile and that part of the MOLA topography, which has not been affected by heavy post-rift modifications (see below). Acceptable fits are obtained for profiles with misfits below 1.5 times the minimum misfit for the flank considered.

[42] The solid line in Figure 14 shows the stacked mean topography of the southern flank as a function of distance along the profiles given in Figure 12. The spread of one standard deviation is indicated by broken lines and results have been smoothed with a moving average with smoothing length 5 km. A global topographic gradient of 5 m km^{-1} has been subtracted. Between 50 and 160 km, the flank has later been strongly modified by tectonic activity connected to the Acheron Fossae 2 system and this part is omitted when calculating the misfit between MOLA and FEM profiles. The best fit FEM profile is given by the bold line and corresponds to T_e = 10.2 km, s = 2500 m and $K = 6.5 \times 10^{-7}$ m^{-1}, the misfit being 24 m per data point. Acceptable fits are obtained for 8.9 km < T_e < 11.3 km and slips between 2300 and 2700 m, the corresponding profiles having curvatures between 5.3×10^{-7} and 8.2×10^{-7} m^{-1}.

[43] Figure 15 shows the mean topography (solid lines) and spread of one standard deviation (dashed lines) for the northern flank. The best fit FEM profile was determined cutting out the region between 300 and 400 km, as this has been filled in with young lavas from the surrounding planes. The best fitting FEM profile has T_e = 10.2 km, s = 2800 m and $K = 7 \times 10^{-7}$ m^{-1}, the misfit being 17 m per data point. The admissible range of elastic thicknesses at this flank is 9.3–11.2 km for extensions between 2600 and 2900 m, the profiles having curvatures between 6×10^{-7} and 8×10^{-7} m^{-1}.

[44] Using the strength envelope formalism, the elastic thicknesses and curvatures may be converted to mechanical thicknesses, yielding T_m = 13.3–17.8 km for the northern and 12.2–18 km for the southern flank, corresponding to thermal gradients of 28–37 and 28–41 K km^{-1}, respectively.

[45] The results are insensitive to the particular choice of Young's modulus and Poisson ratio. Adopting E = 100 GPa and ν = 0.33 results in only minor changes of the reported values within the previously determined error bounds. Incorporating the parts of the topography later modified by the Acheron Fossae 2 system into the fitting procedure results in minor changes to the best fit FEM profile, but increases the range of admissible fits. For the southern flank we obtain T_e = 8–14 km, corresponding to thermal gradients of 21–50 K km^{-1}. However, these fits fail to reproduce the steep flank uplift and are therefore disregarded. The main uncertainty in the heat flow determination is connected to the assumed rheology, as weaker rheologies lead to considerably smaller heat flow values. We have here assumed that the bulk of the Martian crust is basaltic, as is indicated by geochemical evidence [e.g., *Nimmo and Tanaka*, 2005].

7. Discussion

[46] We have estimated the regional thermal gradient at the time of the Acheron Fossae formation by analyzing lithospheric flexure. Thermal gradients may be converted to heat fluxes using Fourier's law: $F = -k\frac{dT}{dz}$, where large uncertainties are connected to the value of the thermal conductivity k, which strongly depends on material properties like porosity and water content. *McGovern et al.* [2004] assume k = 2.5 W m^{-1} K^{-1}, while *Schultz and Watters* [2001] assume a conductivity of 3.2 W m^{-1} K^{-1}. Taking the presence of a top layer of poorly conducting megaregolith into account we adopt a column averaged thermal conductivity of k = 2 W m^{-1} K^{-1} [*Clifford*, 1993; *Squyres et al.*, 1992] and thus obtain heat fluxes in the range of 56–74 and 56–82 mW m^{-2}.

[47] The thermal gradient at rift zones has been previously determined by *Grott et al.* [2005], yielding 27–33 K km^{-1} at the Coracis Fossae at 3.5–3.9 Ga. The values of 28–37 and 28–41 K km^{-1} determined here are consistent with these results, although smaller gradients for the Noachian period have been found elsewhere on Mars ($\frac{dT}{dz}$ = 14–20 [*Schultz and Watters*, 2001] and >20 K km^{-1} [*McGovern et al.*, 2004]). This discrepancy may be explained in terms of the different regional environments considered, as the extended volcanic activity connected to the rift formation process may imply a substantially increased surface heat flow.

[48] Since Acheron Fossae is a narrow rift one may apply the method used by *Grott* [2005] to constrain the crustal thickness at the time of rift formation. Narrow rifting is only compatible with the heat flows determined here if the crust was no thicker than ~50 km when the Acheron Fossae formed. This is consistent with todays crustal thickness value of 45–50 km, as determined by *Neumann et al.* [2004] using gravity and topography data.

[49] On the basis of its topographic expression, overall extensional deformation, and structural features we interpret the Acheron Fossae 1 system to be comparable to terrestrial continental rifts, following the definition of a continental rift by *Olsen and Morgan* [1995] and *Ebinger and Hayward* [1996] (see *Hauber and Kronberg* [2005] for details on these definitions). The dimensions of the length and width of the Acheron Fossae 1 system fall well within the size range of rifts on Earth (compare *Sengör and Natal'in* [2001]), and values of crustal extension across the Acheron Fossae 1 system are comparable to extension across young

terrestrial continental rifts: 1.7–8.7 km for the Acheron Fossae 1 system and 5–10 km for the central Kenya Rift [*Mechie et al.*, 1997].

[50] The observed segmentation along the Acheron Fossae 1 system might have been associated with lateral differences in the thickness of the ancient crust, i.e., a thinning crust along the eastern segment toward Acheron Montes, where magmatism might have been facilitated by a thinned crust. At present, the Acheron Montes are a region of increased crustal thickness with respect to their surroundings [*Neumann et al.*, 2004].

[51] Acheron Fossae and Olympus Mons are located relatively close together, and the long and thin, "banana-shaped" topographic high characterizing the Acheron Fossae region is, at first sight, oriented roughly concentric around the main volcanic shield. Both facts have led to speculations that there might be a causal relationship between both. *McGovern et al.* [1998] and *McGovern* [2002] raised the possibility that the grabens and elevated topography of Acheron Fossae region are the result of ancient loading by Olympus Mons, creating a flexural arch peripheral to Olympus Mons. Since the high topography of Acheron Fossae is an old feature, as indicated by the Hesperian-aged lava flow fronts (see above), and the caldera activity has been recently dated to be as young as ~100–200 Ma [*Neukum et al.*, 2004a], this would indicate a very long history for the volcano. If the high topography of Acheron Fossae, 1200 km apart from the center of Olympus Mons, is indeed caused by flexural loading, a thickness of 75–100 km of the elastic lithosphere is implied [*Solomon et al.*, 1998].

[52] However, it is also possible that the Acheron Fossae topography is not related to Olympus Mons, but is rather an isolated and unrelated ancient structure [*McGovern et al.*, 1998]. We favor this idea based on the following reasons. First, the circle defined by the annular geometry of the high topography of Acheron Fossae is, at close inspection, by no means centered anywhere near the center of the volcanic edifice of Olympus Mons. Instead, the center of such a circle, which has a radius of ~530 km, is located at about 30°N and 225°E, which is halfways between Acheron Fossae and Olympus Mons. This has led *Scott et al.* [1981] and *Morris and Howard* [1981] to suggest that the Acheron Fossae material might represent the remnants of an old shield volcano whose central part has collapsed or subsided, an idea which is also not supported by any of our observations. Second, the volcanic activity in the Acheron Fossae region (see section 4.4) is not readily explained by flexural loading. Finally, the very large thickness of the elastic lithosphere implied by a flexural loading scenario is not in agreement with our results, which indicate a much thinner lithosphere at the end of the Noachian and the Early Hesperian. Furthermore, if lithospheric strength is predominantly carried by the crust, thermochemical evolution models also predict the lithosphere to be thin [*Schumacher and Breuer*, 2006].

[53] We see the extensional tectonics along the east–west trending topographic high of Acheron Fossae as a surface expression of upwelling asthenospheric material and crustal breakup on top of a small diapiric mantle plume that initiated regional uplift, crustal extension and associated volcanic activity in Noachian time. Under this assumption it is of interest that our photogeological mapping indicates that the formation and development of the superimposed NW–SE-trending Acheron Fossae 2 graben system could be the result of tensile stress associated with late-stage crustal uplift around Acheron Dorsum and along the northern part of the western Acheron Fossae 1 segment. We observe that the entire crustal block situated to the southwest of the Acheron Fossae 2 graben system is offset southward by several hundred meters over a length of about 350 km on south and southwest dipping master fault systems that border the western topographic high and Acheron Dorsum toward south and southwest respectively.

8. Conclusion

[54] According to the results of our structural mapping, the rift-like Acheron Fossae 1 system can be observed over a length of about 740 km. Its distinct rift valley changes in width between 45 km and 145 km, spreading eastward. The depths of internally fractured rift grabens reach values over 2.0 km. The lengths of master faults vary between 30 km and 80 km. Extensional structures and the Acheron Fossae 1 rift valley developed along an isolated topographic high about 800 km in length and 170–310 km in width that indicates crustal upwarping. The width of the uplift and the overall elevation of the graben systems increase eastward toward Acheron Montes, which are thought to represent a rift-related center of volcanic activity with elevations up to 3200 m. Along the trend of the rift, one can differentiate the Acheron Fossae 1 system into three parts with respect to lateral changes in width and architecture of extensional faulting. The eastern segment (around 125 km long) is characterized by wide extensional faulting, large throw along several deep and extensive graben structures and rift-related volcanism. The volcanic center, corresponding to the Acheron Montes, is crossed by graben structures. Toward the west, the ~140-km-wide eastern segment narrows down to the discrete axial graben of the central segment, which is around 25 km wide and bordered by step faults. Farther west, the ~225-km-long central segment transforms into the sinuous fault pattern of the western segment with subparallel narrow horst and graben structures, which are 50–60 km wide and 260 km long. This E–W-trending western segment of the Acheron Fossae 1 system is superimposed and displaced vertically by NW–SE trending Acheron Fossae 2 grabens.

[55] Crustal extension as measured along HRSC-derived topographical profiles across the Acheron Fossae 1- graben structures varies from 1.7 km to 8.7 km along the rift trend. In general, the crustal extension increases eastward toward Acheron Montes, together with an increasing width of the rift valley. Strain values vary between 4% and 9%. Measurements across the eastern rift segment reveal that about 44% of the total crustal extension is accommodated by throw on a few large normal border faults.

[56] The volcanic center of Acheron Montes is related to rifting and indicates local magmatic uprise and involvement of the lithosphere. The observed change along the rift trend in topography, fault geometry and crustal extension of the exposed Acheron Fossae 1 system favors westward propagation of rifting from a magma tectonic center Acheron Montes. Our photogeological mapping indicates that the

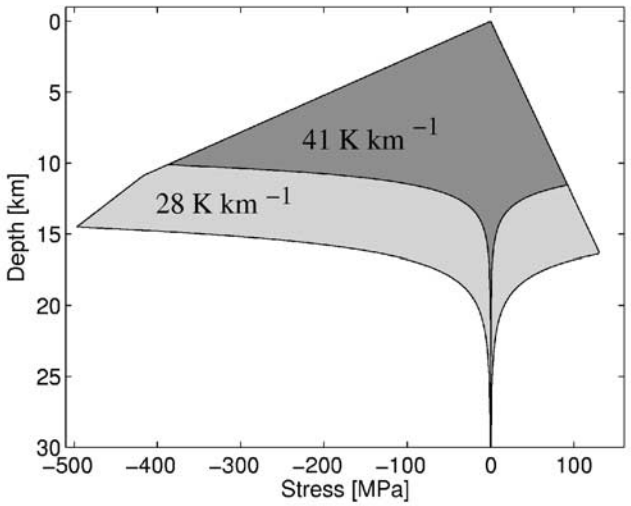

Figure 16. Yield strength envelope for a diabase crust and thermal gradients of 28 and 41 K km^{-1}, as derived for the Martian lithopshere near Acheron Fossae in the late Noachian to early Hesperian periods. Compressional stresses are negative.

Acheron Fossae 1 system might continue eastward under a cover of Hesperian-aged lava flows from Alba Patera. The directional trend of the Acheron Fossae 1 system results from N–S-oriented tensional stress. The Acheron Fossae 1 system does not seem to be part of the radial extensional structures that are related to the Tharsis rise [e.g., *Plescia and Saunders*, 1982]. It might rather be an ancient and isolated feature, comparable to the Coracis Fossae rifts [*Kronberg et al.*, 2006; *Grott et al.*, 2005], which also do not follow a radial orientation to anywhere in Tharsis.

[57] Assuming a diabase composition of the crust, the thermal gradients determined from rift flank uplift at the Acheron Fossae 1 are in the range of 28–41 K km^{-1}. Given a crustal thickness of 45–50 km [*Neumann et al.*, 2004], this implies that the early Martian lithosphere was situated within the crust (see Figure 16). Owing to the high temperatures the mantle carried no strength and its behaviour was governed by ductile flow.

[58] **Acknowledgments.** We thank the HRSC Experiment Teams at DLR Berlin and Freie Universität Berlin as well as the Mars Express Project Teams at ESTEC and ESOC for their successful planning and acquisition of data as well as for making the processed data available to the HRSC Team. We acknowledge the effort of the HRSC Co-Investigator Team members and their associates who have contributed to this investigation in the preparatory phase and in scientific discussions within the Team. SCW acknowledges financial support from the German Research Foundation (DFG) within the priority program SPP 1115 Mars and the Terrestrial Planets. This work was also financially supported by the Federal Ministry of Economics and Technology (BMWI) under contract 50 QM 0404.

References

Anderson, E. M. (1951), *The Dynamics of Faulting and Dyke Formation With Applications to Britain*, 2nd ed., 206 pp., Oliver and Boyd, Edinburgh, U.K.

Anderson, F. S., and R. E. Grimm (1999), Rifting of Valles Marineris, Mars: A finite-element analysis, *Proc. Lunar Planet. Sci. Conf.*, *30th*, abstract 1954.

Anderson, F. S., W. B. Banerdt, and M. P. Golombek (1999), Implications of flexural flanks at the Valles Marineris, Mars, in *5th International Conference on Mars* [CD-ROM], *LPI Contrib. 972*, abstract 6232, Lunar and Planet. Inst., Houston, Tex.

Anderson, R. C., J. M. Dohm, M. P. Golombek, A. F. C. Haldemann, B. J. Franklin, K. L. Tanaka, J. Lias, and B. Peer (2001), Primary centers and secondary concentrations of tectonic activity through time in the western hemisphere of Mars, *J. Geophys. Res.*, *106*, 20,563–20,585.

Anderson, R. C., J. M. Dohm, A. F. C. Haldemann, T. M. Hare, and V. R. Baker (2004), Tectonic histories between Alba Patera and Syria Planum, Mars, *Icarus*, *171*, 31–38.

Anderson, S., and R. E. Grimm (1998), Rift processes at the Valles Marineris, Mars: Constraints from gravity on necking and rate-dependent strength evolution, *J. Geophys. Res.*, *103*, 11,113–11,124.

Banerdt, W. B., M. P. Golombek, and K. L. Tanaka (1992), Stress and tectonics on Mars, in *Mars*, edited by H. H. Kieffer et al., pp. 249–297, Univ. of Ariz. Press, Tucson.

Barnett, D. N., and F. Nimmo (2002), Strength of faults on Mars from MOLA topography, *Icarus*, *157*, 34–42.

Brown, C. D., and R. J. Phillips (1999), Flexural rift flank uplift at the Rio Grande Rift, New Mexico, *Tectonics*, *18*, 1275–1291.

Byerlee, J. D. (1978), Friction of rocks, *Pure Appl. Geophys.*, *116*, 615–626.

Cailleau, B., T. R. Walter, P. Janle, and E. Hauber (2005), Unveiling the origin of radial grabens on Alba Patera volcano by finite element modeling, *Icarus*, *176*, 44–56.

Caristan, Y. (1982), The transition from high temperature creep to fracture in Maryland diabase, *J. Geophys. Res.*, *87*, 6781–6790.

Chéry, J., F. Lucazeau, M. Daignières, and J. P. Vilotte (1992), Large uplift of rift flanks: A genetic link with lithospheric rigidity?, *Earth Planet. Sci. Lett.*, *112*, 195–211.

Chuang, F. C., and D. A. Crown (2005), Surface characteristics and degradational history of debris aprons in the Tempe Terra/Mareotis fossae region of Mars, *Icarus*, *179*, 24–42.

Clifford, S. M. (1993), A model for the hydrologic and climatic behavior of water on Mars, *J. Geophys. Res.*, *98*, 10,973–11,016.

Clifford, S. M., and T. J. Parker (2001), The evolution of the Martian hydrosphere: Implications for the fate of a primordial ocean and the current state of the Northern Plains, *Icarus*, *154*, 40–79.

Ebinger, C. J., and N. J. Hayward (1996), Soft plates and hot spots: Views from afar, *J. Geophys. Res.*, *101*, 21,859–21,876.

Forget, F., R. M. Haberle, F. Montmessin, B. Levrard, and J. W. Head (2006), Formation of glaciers on Mars by atmospheric precipitation at high obliquity, *Science*, *311*, 368–371.

Frey, H. (1979), Martian canyons and African rifts: Structural comparisons and implications, *Icarus*, *37*, 142–155.

Golombek, M. P., K. L. Tanaka, and B. J. Franklin (1996), Extension across Tempe Terra, Mars, from measurements of fault scarp widths and deformed craters, *J. Geophys. Res.*, *101*, 26,119–26,130.

Grott, M. (2005), Late crustal growth on Mars: Evidence from lithospheric extension, *Geophys. Res. Lett.*, *32*, L23201, doi:10.1029/2005GL024492.

Grott, M., E. Hauber, S. C. Werner, P. Kronberg, and G. Neukum (2005), High heat flux on ancient Mars: Evidence from rift flank uplift at Coracis Fossae, *Geophys. Res. Lett.*, *32*, L21201, doi:10.1029/2005GL023894.

Gwinner, K., F. Scholten, B. Giese, J. Oberst, R. Jaumann, M. Spiegel, R. Schmidt, and G. Neukum (2005), Hochauflösende Digitale Geländemodelle auf der Grundlage von Mars Express HRSC-Daten, *Photogramm. Fernerkund. Geoinf.*, *2005/5*, 387–394.

Harrington, B. W., R. J. Phillips, and M. P. Golombek (1999), Extension across Tempe Terra, Mars from MOLA topographic measurements, in *Fifth International Conference on Mars* [CD-ROM], *LPI Contrib. 972*, abstract 6130, Lunar and Planet. Inst., Houston, Tex.

Hartmann, W. K., and G. Neukum (2001), Cratering chronology and the evolution of Mars, *Space Sci. Rev.*, *96*, 165–194.

Hauber, E., and P. Kronberg (2001), Tempe Fossae, Mars: A planetary analogon to a terrestrial continental rift?, *J. Geophys. Res.*, *106*, 20,587–20,602.

Hauber, E., and P. Kronberg (2005), The large Thaumasia graben on Mars: Is it a rift?, *J. Geophys. Res.*, *110*, E07003, doi:10.1029/2005JE002407.

Hauber, E., et al. (2005), Discovery of a flank caldera and very young glacial activity at Hecates Tholus, Mars, *Nature*, *434*, 356–361.

Head, J. W., A. L. Nahm, D. R. Marchant, and G. Neukum (2006), Modification of the dichotomy boundary on Mars by Amazonian mid-latitude regional glaciation, *Geophys. Res. Lett.*, *33*, L08S03, doi:10.1029/2005GL024360.

Komatsu, G. (2003), Geological processes in the Baikal Rift zone: Potential terrestrial analogs for the Valles Marineris region on Mars, *Proc. Lunar Planet. Sci. Conf.*, *34th*, abstract 1314.

Kronberg, P., E. Hauber, K. Gwinner, B. Giese, T. Schäfer, P. Masson, G. Neukum, and the HRSC Co-Investigator Team (2005), Acheron Fossae, Mars: A Martian rift observed by the High Resolution Stereo Camera (HRSC), *Geophys. Res. Abstr.*, *7*, 04244.

Kronberg, P., E. Hauber, T. Schäfer, M. Grott, S. C. Werner, K. Gwinner, and P. Masson (2006), The double rift system of Coracis Fossae—A

specific style of crustal extension on early Mars?, *Geophys. Res. Abstr.*, *8*, 01607.
Li, H., M. S. Robinson, and D. M. Jurdy (2005), Origin of Martian northern hemisphere mid-latitude lobate debris aprons, *Icarus*, *176*, 382–394.
Lucchitta, B. K. (1984), Ice and debris in the fretted terrain, Mars, *Proc. Lunar Sci. Conf. 14th*, Part 2, *J. Geophys. Res.*, *89*, suppl., B409–B418.
Malin, M. C., and K. S. Edgett (1999), Oceans or seas in the Martian northern lowlands: High resolution imaging tests of proposed coastlines, *Geophys. Res. Lett.*, *26*, 3049–3052.
Malin, M. C., and K. S. Edgett (2001), Mars Global Surveyor Mars Orbiter Camera: Interplanetary cruise through primary mission, *J. Geophys. Res.*, *106*, 23,429–23,570.
Malin, M. C., G. E. Danielson, A. P. Ingersoll, H. Masursky, J. Veverka, M. A. Ravine, and T. A. Soulanille (1992), Mars Observer Camera, *J. Geophys. Res.*, *97*, 7699–7718.
Masson, P. (1977), Structure pattern analysis of the Noctis Labyrinthus–Valles Marineris regions of Mars, *Icarus*, *30*, 49–62.
Masson, P. (1980), Contribution to the structural interpretation of the Valles Marineris–Noctis Labyrinthus–Claritas Fossae regions of Mars, *Moon Planets*, *22*, 211–219.
Masson, P. (1985), Origin and evolution of the Valles Marineris region of Mars, *Adv. Space Res.*, *50*, 83–92.
McGovern, P. J. (2002), Interpretations of gravity anomalies at Olympus Mons, Mars: Intrusions, impact basins, and troughs, *Proc. Lunar Planet. Sci. Conf.*, *33th*, abstract 2024.
McGovern, P. J., C. L. Johnson, S. S. Solomon, J. W. Head, W. B. Banerdt, M. T. Zuber, D. E. Smith, and R. J. Phillips (1998), Lithospheric loading and evolution of large volcanoes on Mars: New insights from MOLA observations, *Proc. Lunar Planet. Sci. Conf.*, *29th*, abstract 1238.
McGovern, P. J., S. C. Solomon, D. E. Smith, M. T. Zuber, M. Simons, M. A. Wieczorek, R. J. Phillips, G. A. Neumann, O. Aharonson, and J. W. Head (2002), Localized gravity/topography admittance and correlation spectra on Mars: Implications for regional and global evolution, *J. Geophys. Res.*, *107*(E12), 5136, doi:10.1029/2002JE001854.
McGovern, P. J., S. C. Solomon, D. E. Smith, M. T. Zuber, M. Simons, M. A. Wieczorek, R. J. Phillips, G. A. Neumann, O. Aharonson, and J. W. Head (2004), Correction to "Localized gravity/topography admittance and correlation spectra on Mars: Implications for regional and global evolution," *J. Geophys. Res.*, *109*, E07007, doi:10.1029/2004JE002286.
McNutt, M. K. (1984), Lithospheric flexure and thermal anomalies, *J. Geophys. Res.*, *89*, 11,180–11,194.
Mechie, J., G. R. Keller, C. Prodehl, M. A. Khan, and S. J. Gaciri (1997), A model for the structure, composition and evolution of the Kenya Rift, *Tectonophysics*, *278*, 95–119.
Mège, D., and P. Masson (1996), Amounts of crustal stretching in the Valles Marineris, Mars, *Planet. Space Sci.*, *44*, 749–782.
Milliken, R. E., J. F. Mustard, and D. L. Goldsby (2003), Viscous flow features on the surface of Mars: Observations from high-resolution Mars Orbiter Camera (MOC) images, *J. Geophys. Res.*, *108*(E6), 5057, doi:10.1029/2002JE002005.
Morris, E. C., and K. A. Howard (1981), Geologic map of the Diacria Quadrangle of Mars, scale 1:5,000,000, *U.S. Geol. Surv. Misc. Invest. Ser.*, *Map I-1286*.
Morris, E. C., and K. L. Tanaka (1994), Geologic maps of the Olympus Mons region of Mars, scale 1:2,000,000, *U.S. Geol. Surv. Misc. Invest. Ser.*, *Map I-2327*.
Mueller, S., and R. J. Phillips (1995), On the reliability of lithospheric constraints derived from models of outer-rise flexure, *Geophys. J. Int.*, *123*, 887–902.
Mustard, J. F., C. D. Cooper, and M. K. Rifkin (2001), Evidence for recent climate change on Mars from the identification of youthful near- surface ground ice, *Nature*, *412*, 411–414.
Neukum, G., and K. Hiller (1981), Martian ages, *J. Geophys. Res.*, *86*, 3097–3121.
Neukum, G., et al. (2004a), Recent and episodic volcanic and glacial activity on Mars revealed by the High Resolution Stereo Camera, *Nature*, *432*, 971–979.
Neukum, G., R. Jaumann, and the HRSC Co-Investigator and Experiment Team (2004b), HRSC: The High Resolution Stereo Camera of Mars Express, *ESA SP-1240*, pp. 17–35, Eur. Space Agency, Noordwijk, Netherlands.
Neumann, G. A., M. T. Zuber, M. A. Wieczorek, P. J. McGovern, F. G. Lemoine, and D. E. Smith (2004), Crustal structure of Mars from gravity and topography, *J. Geophys. Res.*, *109*, E08002, doi:10.1029/2004JE002262.
Nimmo, F., and K. Tanaka (2005), Early crustal evolution of Mars, *Annu. Rev. Earth Planet. Sci.*, *33*, 133–161.
Olsen, K. H., and P. Morgan (1995), Introduction: Progress in understanding continental rifts, in *Continental Rifts: Evolution, Structure, Tectonics*, edited by K. H. Olsen, pp. 3–26, Elsevier, New York.
Parker, T. J., R. S. Saunders, and D. M. Schneeberger (1989), Transitional morphology in west Deuteronilus Mensae, Mars—Implications for modification of the lowland/upland boundary, *Icarus*, *82*, 111–145.
Plescia, J. B., and R. S. Saunders (1982), Tectonic history of the Tharsis region, Mars, *J. Geophys. Res.*, *87*, 9775–9791.
Schoenfeld, E. (1979), Origin of Valles Marineris, *Proc. Lunar Planet. Sci. Conf., 10th*, Part 3, *J. Geophys. Res.*, *84*, suppl., 3031–3039.
Scholten, F., K. Gwinner, T. Roatsch, K.-D. Matz, M. Waehlisch, B. Giese, J. Oberst, R. Jaumann, G. Neukum, and the HRSC Co-Investigator Team (2005), Mars Express HRSC data processing—Methods and operational aspects, *Photogramm. Eng. Remote Sens.*, *71*, 1143–1152.
Schultz, R. A. (1991), Structural development of Coprates Chasma and western Ophir Planum, Valles Marineris rift, Mars, *J. Geophys. Res.*, *96*, 22,777–22,792.
Schultz, R. A. (1995), Gradients in extension and strain at Valles Marineris, Mars, *Planet. Space Sci.*, *43*, 1561–1566.
Schultz, R. A., and T. R. Watters (2001), Forward mechanical modeling of the Amenthes Rupes thrust fault on Mars, *Geophys. Res. Lett.*, *28*, 4659–4662.
Schumacher, S., and D. Breuer (2006), Influence of a variable thermal conductivity on the thermochemical evolution of Mars, *J. Geophys. Res.*, *111*, E02006, doi:10.1029/2005JE002429.
Scott, D. H. (1982a), Volcanoes and volcanic provinces: Martian western hemisphere, *J. Geophys. Res.*, *87*, 9839–9851.
Scott, D. H. (1982b), Mars—A large highland volcanic province revealed by Viking images, *Proceedings of the 12th Lunar and Planetary Science Conference*, pp. 1449–1458, Elsevier, New York.
Scott, D. H., and M. H. Carr (1978), Geologic map of Mars, scale 1:25,000,000, *U.S. Geol. Surv. Misc. Invest. Ser.*, *Map I-1083*.
Scott, D. H., and K. L. Tanaka (1986), Geologic map of the western equatorial region of Mars, scale 1:15,000,000, *U.S. Geol. Surv. Misc. Invest. Ser.*, *Map I-1802-A*.
Scott, D. H., G. G. Schaber, K. L. Tanaka, K. C. Horstman, and A. L. Dial (1981), Map series showing lava-flow fronts in the Tharsis region of Mars, scale 1:5,000,000, *U.S. Geol. Surv. Misc. Invest. Ser.*, *Map I-1266–I-1280*.
Sengör, A. M., and B. A. Natal'in (2001), Rifts of the world, in *Mantle Plumes: Their Identification Through Time*, edited by R. E. Ernst and K. L. Buchan, *Spec. Pap. 352*, pp. 389–482, Geol. Soc. of Am., Boulder, Colo.
Smith, D. E., et al. (2001), Mars Orbiter Laser Altimeter: Experiment summary after the first year of global mapping of Mars, *J. Geophys. Res.*, *106*, 23,689–23,722.
Sohl, F., G. Schubert, and T. Spohn (2005), Geophysical constraints on the composition and structure of the Martian interior, *J. Geophys. Res.*, *110*, E12008, doi:10.1029/2005JE002520.
Solomon, S. C., C. L. Johnson, P. J. McGovern, O. Aharonson, W. B. Banerdt, J. W. Head, R. J. Phillips, D. E. Smith, and M. T. Zuber (1998), An overview of lithospheric flexure on Mars: Implications of initial MOLA observations, *Proc. Lunar Planet. Sci. Conf.*, *29th*, abstract 1389.
Squyres, S. W. (1978), Martian fretted terrain: Flow of erosional debris, *Icarus*, *34*, 600–613.
Squyres, S. W. (1979), Distribution of lobate debris aprons and similar flows on Mars, *J. Geophys. Res.*, *84*, 8087–8096.
Squyres, S. W., S. M. Clifford, R. O. Kuzmin, J. R. Zimbelman, and F. M. Costard (1992), Ice in the Martian regolith, in *Mars*, edited by H. H. Kieffer et al., pp. 523–554, Univ. of Ariz. Press, Tucson.
Tanaka, K. L. (1983), Geology of the Olympus Mons region of Mars, Ph.D. dissertation, map scale 1:3,000,000, 264 pp., Univ. of Calif., Santa Barbara.
Tanaka, K. L., M. P. Golombek, and W. B. Banerdt (1991), Reconciliation of stress and structural histories of the Tharsis region of Mars, *J. Geophys. Res.*, *96*, 15,617–15,633.
Tanaka, K. L., J. A. Skinner, and T. M. Hare (2005), Geologic map of the Northern Plains of Mars, scale 1:15,000,000, *U.S. Geol. Surv. Sci. Invest.*, *Map 2888*.
Upcott, N. M., R. K. Mukasa, C. J. Ebinger, and G. D. Karner (1996), Along-axis segmentation and isostasy in the Western rift, East Africa, *J. Geophys. Res.*, *101*, 3247–3268.
Watters, T. R., R. A. Schultz, M. S. Robinson, and A. C. Cook (2002), The mechanical and thermal structure of Mercury's early lithosphere, *Geophys. Res. Lett.*, *29*(11), 1542, doi:10.1029/2001GL014308.
Weissel, J. K., and G. D. Karner (1989), Flexural uplift of rift flanks due to mechanical unloading of the lithosphere during extension, *J. Geophys. Res.*, *94*, 13,919–13,950.
Werner, S. C. (2005), Major aspects of the chronostratigraphy and geologic evolutionary history of Mars, Ph.D. thesis, 252 pp., Freie Univ., Berlin. (Available at http://www.diss.fu-berlin.de/2006/33/indexe.html)
Wood, C. A., and J. W. Head (1978), Rift valleys on Earth, Mars, and Venus, in *Tectonics and Geophysics of Continental Rifts*, edited by I. B. Ramberg and E. R. Neumann, pp. 401–408, Springer, New York.

Zuber, M. T., D. E. Smith, S. C. Solomon, D. O. Muhleman, J. W. Head, J. B. Garvin, J. B. Abshire, and J. L. Bufton (1992), The Mars Observer Laser Altimeter Investigation, *J. Geophys. Res.*, *97*, 7781–7797.

B. Giese, M. Grott, K. Gwinner, and E. Hauber, Institute of Planetary Research, German Aerospace Center (DLR), Rutherfordstr. 2, D-12489 Berlin, Germany. (bernd.giese@dlr.de; matthias.grott@dlr.de; klaus.gwinner@dlr.de; ernst.hauber@dlr.de)

P. Kronberg and T. Schäfer, Institute of Geology and Paleontology, Technical University Clausthal, Leibnizstr. 10, D-38678 Clausthal-Zellerfeld, Germany. (peter.kronberg@tu-clausthal.de; tanja.schaefer@tu-clausthal.de)

P. Masson, Laboratoire Orsayterre (CNRS FRE 2566), Université Paris-Sud (bat. 509), F-91405 Orsay Cedex, France. (masson@geol.u-psud.fr)

G. Neukum and S. C. Werner, Institute of Geosciences, FU Berlin, Malteser Str. 74-100, D-12249 Berlin, Germany. (gneukum@zedat.fu-berlin.de; swerner@zedat.fu-berlin.de)